Harmful Algae 127 (2023) 102475

Contents lists available at ScienceDirect

Harmful Algae

journal homepage: www.elsevier.com/locate/hal

Thecal plate morphology, molecular phylogeny, and toxin analyses reveal two novel species of *Alexandrium* (Dinophyceae) and their potential for toxin production

Nursyahida Abdullah [a], Sing Tung Teng [a,*], Afiqah Hamilton Hanifah [a], Ing Kuo Law [b], Toh Hii Tan [c], Bernd Krock [d], Thomas M. Harris [e,f], Satoshi Nagai [g], Po Teen Lim [b], Urban Tillmann [d], Chui Pin Leaw [b,**]

[a] Faculty of Resource Science and Technology, Universiti Malaysia Sarawak, 94300, Kota Samarahan, Sarawak, Malaysia
[b] Bachok Marine Research Station, Institute of Ocean and Earth Sciences, University of Malaya, 16310 Bachok, Kelantan, Malaysia
[c] Department of Animal Science and Fishery, Faculty of Agricultural Science and Forestry, Universiti Putra Malaysia, 97008, Bintulu, Sarawak, Malaysia
[d] Section Ecological Chemistry, Alfred Wegener Institute, Helmholtz Centre for Polar and Marine Research, 27570, Bremerhaven, Germany
[e] Department of Chemistry, Vanderbilt, University, Nashville, Tennessee, 37235, United States
[f] Virginia Institute of Marine Science (VIMS), Gloucester Point, Virginia, 23062, United States
[g] Japan Fisheries Research and Education Agency, 2-12-4 Fukuura, Kanazawa, Yokohama, Kanagawa 236-8648, Japan

ARTICLE INFO

Editor: Dr. C. Gobler

Keywords:
Alexandrium
Goniodomins
Harmful algal bloom
ITS secondary structure
Paralytic shellfish toxins
Taxonomy
Thecal plates

ABSTRACT

This study describes two novel species of marine dinophytes in the genus *Alexandrium*. Morphological characteristics and phylogenetic analyses support the placement of the new taxa, herein designated as *Alexandrium limii* sp. nov. and *A. ogatae* sp. nov. *Alexandrium limii*, a species closely related to *A. taylorii*, is distinguished by having a shorter 2'/4' suture length, narrower plates 1' and 6", with larger length: width ratios, and by the position of the ventral pore (Vp). *Alexandrium ogatae* is distinguishable with its metasert plate 1' having almost parallel lateral margins, and by lacking a Vp. Production of paralytic shellfish toxins (PSTs), cycloimines, and goniodomins (GDs) in clonal cultures of *A. ogatae, A. limii*, and *A. taylorii* were examined analytically and the results showed that all strains contained GDs, with GDA as major variants (6–14 pg cell^{-1}) for all strains except the Japanese strain of *A. limii*, which exclusively had a desmethyl variant of GDA (1.4–7.3 pg cell^{-1}). None of the strains contained detectable levels of PSTs and cycloimines.

1. Introduction

The genus *Alexandrium* Halim is a marine dinophyte commonly found in coastal waters around the world (Hallegraeff, 1993; Anderson et al., 2012). *Alexandrium* has been extensively studied in recent decades for its ability to produce paralytic shellfish toxins (PSTs) in several toxigenic species. PSTs are a group of potent neurotoxins also known as saxitoxin (STX) variants. The toxin accumulates in shellfish vectors, transfers to humans, and causes severe neurological symptoms, including paralysis and respiratory failure, causing paralytic shellfish poisoning (PSP). Of the 32 taxonomically accepted species to date (Mertens et al., 2020), 16 are listed as harmful species (Lundholm et al., 2023), at least one-third are capable to produce PSP toxins. In recent decades, there have been numerous PSP outbreaks worldwide, particularly in Southeast Asia, resulting in human fatalities (e.g., Lim et al., 2007, 2012, 2020; Yñiguez et al., 2021). Furthermore, blooms of several *Alexandrium* species are known to cause significant losses to aquaculture industries in America, Europe, Asia (Trainer and Yoshida, 2014; Trainer, 2020), Australia, and New Zealand (MacKenzie et al., 2004; Jin et al., 2008; Condie et al., 2019). To cite an instance, the 2016 bloom of *A. catenella* (Whedon & Kofoid) Balech in Chile was a notable case that badly hit the salmon aquaculture industries. This bloom killed over 30, 000 tons of farmed salmon, causing losses of over $800 million (Díaz et al., 2019). There are several species of *Alexandrium* that produce harmful metabolites other than PSTs, such as cycloimines (spirolides, gymnodimines), goniodomins, and some poorly characterized lytic

* Corresponding author.
** Corresponding author.
E-mail addresses: tsteng@unimas.my (S.T. Teng), cpleaw@um.edu.my (C.P. Leaw).

https://doi.org/10.1016/j.hal.2023.102475
Received 25 April 2023; Received in revised form 22 June 2023; Accepted 29 June 2023
Available online 1 July 2023

compounds, which are believed to release into the marine environment and affect a wide range of marine organisms including fishes (reviewed in Long et al., 2021).

Species delineation in *Alexandrium* traditionally relied on distinct features in the thecal plate morphology. For example, the first and third apical plates (1', 3'), the sixth precingular plate (6"), and the sulcal plates are among the plates used to delineate species of *Alexandrium* (Balech, 1985, 1995). Some of these characters, however, have been regarded as labile and taxonomically uninformative (e.g., Delgado et al., 1997; Hansen et al., 2003; Leaw et al., 2005; Kremp et al., 2014; John et al., 2014). Integrative taxonomy based on multiple lines of evidence encompassing morphology, molecular phylogenies, and mating compatibility has been increasingly applied in dinophyte taxonomy. The molecular phylogenetic approach has become one of the most widely accepted approaches to affirm the species validity of *Alexandrium*. Among the numerous genetic markers, the nuclear-encoded ribosomal DNAs (SSU, ITS, and LSU rDNA) have been widely used to infer the phylogenetic relationships of the species in *Alexandrium* (Usup et al., 2002; Leaw et al., 2005; Lilly et al., 2007; Gu et al., 2013; John et al., 2014; Kremp et al., 2014; Branco et al., 2020; Tillmann et al., 2021). Integrating both the morphology and molecular characteristics of species in the genus has proven powerful in delineating the species boundaries in some studies (Fraga et al., 2015; Litaker et al., 2018).

In *Alexandrium* taxonomy, species that share a metasert or exsert plate 1' (not rhomboidal/insert) which is constantly disconnected from the apical pore plate (Po), were classified in the subgenus *Gessnerium sensu* Balech (1995). Balech chose this subgenus name based on the heterotypic junior synonym (*Gessnerium mochimaense* Halim) of the first described species of this group (*Alexandrium monilatum* (J.F.Howel) Balech). The nine species assigned to *Gessnerium* by Balech (1995) are *A. balechii* (Steidinger) Balech, *A. foedum* Balech, *A. hiranoi* K.Kita & Y. Fukuyo, *A. insuetum* Balech, *A. margalefii* Balech, *A. monilatum, A. pseudogonyaulax* (Biecheler) Horiguchi ex K.Yuki & Y.Fukuyo, *A. satoanum* K.Yuki & Y.Fukuyo, and *A. taylorii* Balech. Other species described later with the *Gessnerium*-type 1' include *A. camurascutulum* MacKenzie & K.Todd, *A. concavum* (Gaarder) Balech emend. Nguyen Ngoc & Larsen, *A. globosum* Nguyen-Ngoc & J.Larsen, and *A. pohangense* A.S.Lim & H.J.Jeong. The morphological concept of Balech (1995) in differentiating between the subgenera *Alexandrium* and *Gessnerium* somehow failed to reflect two distinct genetically inferred evolutionary units. Several species of the subgenus *Gessnerium sensu* Balech (*A. hiranoi, A. monilatum, A. pseudogonyaulax, A. satoanum, A. taylorii*) formed a highly supported monophyletic clade (a *Gessnerium* clade), but several species, for instance, *A insuetum, A. margalefii*, and *A. pohangense* were grouped with other species in the subgenus *Alexandrium sensu* Balech in the rDNA phylogenetic trees (Kim et al., 2005; Leaw et al., 2005; Tillmann et al., 2021). From a chemical perspective, species of the *Gessnerium* clade are known to produce goniodomin A (GDA), this includes *A. hiranoi, A. monilatum, A. pseudogonyaulax*, and *A. taylorii* (e.g., Hsia et al., 2006; Espina et al., 2016; Triki et al., 2016; Krock et al., 2018; Tillmann et al., 2020). Although little is known about their toxicity potentials and impacts on ecology and socio-economy (Tillmann et al., 2020), it was shown that GDs can cause liver and thymus damage in mice (Terao et al., 1989), are cytotoxic (Espiña et al., 2016), and have been associated with mortality in aquatic invertebrates (Harding et al., 2009), with significant impacts on local ecosystems.

For identification of the full species diversity within this *Gessnerium* clade, there is a need to re-examine and integrate molecular information of the other described species with a *Gessnerium*-type 1' plate (e.g., *A. balechii, A. camurascutulum, A. concavum, A. foedum, A. globosum*). Moreover, large differences in the GenBank sequence entries annotated as *A. taylorii* indicate the possibility of multiple distinct lineages (Tillmann et al., 2020). A morphospecies that resembled *A. taylorii* was reported by Lim et al. (2005) from Malaysian Borneo; the strains were previously designated as *A. taylorii* based on the thecal morphology that resembled the species (Balech, 1995). But no molecular data from the strains were available at that time for phylogenetic inference. In the present study, the site where the strains were isolated was revisited, and new strains were established in culture. Together, several *Alexandrium* strains from different geographical regions were also established and examined for species identification. Integrating the morphological and molecular evidence in this study revealed two novel species of *Alexandrium*. Further, the presence of relevant toxins for different strains of both new species was determined.

2. Materials and methods

2.1. Algal cultures

Plankton samples were collected by 20-μm mesh plankton net hauls. Live samples were brought back to the laboratory for culture establishment. Single *Alexandrium*-like cells were isolated using a finely drawn Pasteur pipette under an Olympus IX51 inverted light microscope (Olympus, Tokyo, Japan) and transferred to a 96-well tissue culture plate containing GPM medium (Loeblich, 1975).

Malaysian strains were grown in a sterile natural seawater base (salinity of 30) enriched with L1 medium, while strains AY1T, AY7T, and Atay99Shio-02 were grown using a K-based medium (Keller et al., 1987) prepared from 0.2 μm sterile-filtered North Sea water (salinity of 33). The original K-medium receipt was slightly modified by replacing the organic phosphorous source (β-Glycerophosphate) with 3.62 μM disodium hydrogen phosphate (Na_2HPO_4). Strains were grown at 20 °C (AY1T, AY7T), 25 °C (Atay99Shio-02), or 26 °C (Malaysian strains) under moderate photon flux densities (80 μmol photons m^{-2} s^{-1}) at a 16:8 h (temperate strains) or 12:12 h (tropical strains) light:dark cycle in a controlled environment growth chamber (MIR 252, Sanyo Biomedical, Wood Dale, USA or SRI21D-2 Shel Lab, Sheldon Manufacturing, CA, USA).

All *Alexandrium* strains used in this study, with their strain codes and locality, are listed in Table 1.

2.2. Morphological observation

2.2.1. Light microscopy (LM)

Live cells (7–10 days cultures) were examined under an IX51 inverted microscope (Olympus, Tokyo, Japan) or Axiovert 2 microscope (Zeiss, Göttingen, Germany) equipped with epifluorescence and differential interference contrast optics. Images of cells were captured by an INFINITY-3 digital camera (Teledyne Lumenera, Ottawa, Canada) or Axiocam MRc5 (Zeiss) digital camera to record cell shape, and nuclei position and shape.

To determine the shape and position of the nucleus, the culture samples were stained with 0.1% SYBR Safe DNA stain (Invitrogen, MA, USA) in the dark and observed immediately using the same microscope equipped with 450–490 nm excitation and 510–550 nm emission. To observe thecal plate arrangement, cells were stained with Solophenyl Flavine 7GFE (Direct Yellow 96, Sigma-Aldrich, MO, USA), then examined under the microscope with 450–490 nm excitation and 510–550 nm emission.

2.2.2. Scanning electron microscopy (SEM)

Cells were preserved in acidic Lugol's solution with a final concentration of 1%. The preserved cells were filtered on a 3 μm-pore size polycarbonate membrane (Whatman, USA) and washed with distilled water twice for 20 min each. The samples were then dehydrated in a graded ethanol series (30%, 50%, 75%, 90%, 95%, 99%, 99.5%, 15 min at each step; followed by 2 × 99.5%, 2 × 100%, 30 min). The samples were dried using a K580 Critical Point Dryer (Quorum Technologies Ltd., UK). The membrane was mounted on a stub and coated with platinum-palladium using a JEC-3000FC Auto Fine Coater (JEOL, Tokyo, Japan). Cells were examined using a JSM-IT500HR Scanning Electron Microscope (JEOL, Tokyo, Japan).

Table 1
Information of *Alexandrium* species and strains used in this study, including locations, date of collection, temperature and salinity of culture condition, morphological and toxicity information, GenBank accession numbers of the SSU, LSU, and ITS rDNA sequences, and references. *, type specimen. +, morphology/toxicity tested; –, morphology/toxicity not tested.

Species	Strain	Location	Date of collection	Temperature/ salinity	Morphology/ Toxicity	GenBank accession number SSU	LSU	ITS	Reference
A. limii	DBS08 *	Batang Salak (Malaysia) 1° 36′ 31.4886″ N, 110° 19′ 36.6774″ E	Mar 2017	26 °C/ 30	+/+	OP782553	OK271124	OK274344	This study
A. limii	DBS28	Batang Salak (Malaysia) 1° 36′ 31.4886″ N, 110° 19′ 36.6774″ E	Mar 2017	26 °C/ 30	+/–	OP782554	OK271125	OK274343	This study
A. limii	Atay99Shio-02	Shioya Bay, Okinawa (Japan)	Jul 1999	20 °C/ 32	+/+	LC770197	AB607264	LC770198	This study; Nagai and Itakura, 2012
	Atay99Shio-01	Shioya Bay, Okimawa (Japan)	Jul 1999	20 °C/ 32	–/–	–	AB607263	–	This study; Nagai and Itakura, 2012
	Atay99Shio-03	Shioya Bay, Okinawa (Japan)	Jul 1999	20 °C/ 32	–/–	–	AB607265	–	This study; Nagai and Itakura, 2012
	Atay99Shio-06	Shioya Bay, Okinawa (Japan)	Jul 1999	20 °C/ 32	–/–	–	–	AB841262	This study; Nagai, 2013
A. ogatae	LASpbB10 *	Sepanggar Bay (Malaysia) 6° 5′ 29.3388″ N, 116° 7′ 39.2772″ E	Sep 2018	26 °C/ 30	+/+	OP782555	OK271127	OK274341	This study
A. ogatae	LASpbB5	Sepanggar Bay (Malaysia) 6° 5′ 29.3388″ N, 116° 7′ 39.2772″ E	Aug 2018	26 °C/ 30	–/–	–	OK271126	OK274342	This study
A. ogatae	LASpbD3	Sepanggar Bay (Malaysia) 6° 5′ 29.3388″ N, 116° 7′ 39.2772″ E	Sep 2018	26 °C/ 30	+/+	OP782556	OK271128	OK274340	This study
A. pseudogonyaulax	LMIAE9	Lumut (Malaysia) 4°12′35.2″N, 100°36′02.6″E	Oct 2017	26 °C/ 30	+/–	–	OK271130	OK274338	This study
A. pseudogonyaulax	LATAG8	Telaga Air (Malaysia) 1°40′35.6″N, 110°12′35.3″E	Aug 2018	26 °C/ 30	+/–	–	OK271129	OK274339	This study
A. taylorii	AY1T	Lagoon of Marano (Italy)		20 °C/ 32	+/+	AJ535390	AJ535347	–	This study; Tillmann and John, 2002
A. taylorii	AY7T	Lagoon of Marano (Italy)		20 °C/ 32	+/+	–	MT643180	MT644478	This study; Tillmann et al., 2020

2.2.3. Morphometric data analysis

Morphometric measurements of cell dimension and thecal plates were performed on individual cells of nine strains of *Alexandrium* based on the light and SEM micrographs (Table 1). To explore if thecal morphometrics of *Alexandrium* species in this study exhibit differences among strains and species, and to visualize patterns of variations, the dataset was analyzed by using principal component analysis (PCA) as implemented in FactoMineR in R (Lê et al., 2008). The dataset contained 512 cells and 11 morphological variables: cell length (L), cell width (W), L:W, 1' length, 1' width, 1' L:W, 6" length, 6" width, 6" L:W, length of suture adjoined 2' and 4' (herein referred 2'/4' suture), and the ratio of 2'/4' suture to 1' length (Suppl. Material 1).

2.3. Molecular characterization

2.3.1. Genomic DNA isolation, gene amplification, and sequencing

Genomic DNA was isolated from the exponential-phased cultures (7–10 days cultures). Cells were harvested by centrifugation (2800 × *g*, 20 min) and DNA was isolated using the Dneasy® Plant Mini Kit (Qiagen, Hilden, Germany) following the manufacturer's protocol. The purified DNA was kept at −20 °C until further analysis.

The small subunit (SSU) ribosomal RNA gene (rDNA) was amplified using two primer pairs: 18SAlexF1 (5' GCTTGTCTCAAAGATTAAGCC ATGC 3') and 18SAlexR1 (5' CATCCTTGGCAAATGCTTTCGCA 3'); 18SAlexF2 (5' GTCAGAGGTGAAATTCTTGGATT 3') and18SAlexR2 (5' CCTTGTTACGACTTCTCCTTCCTC 3'). The large subunit (LSU) rDNA in the domain D1–D3 was amplified using the primer pair, D1R and D3Ca (Scholin et al., 1994). The internal transcribed spacers (ITS) region was amplified using the primer pair, AlexITSf1 (5' GAGGAAGGAGAAGTC GTAACAAGG 3') and AlexITSr1 (5' CATTCCAATGCCRAGGARTG 3'). The amplifications were carried out in a 25 μL reaction mixture containing 1 × PCR buffer (Promega, Madison, WI, USA), 1.5 mM $MgCl_2$ (Promega), 0.2 mM of dNTPs (Fermentas, Thermo Fisher Scientific, MA, USA), 0.5 μM of each primer, 1 U *Taq* DNA polymerase (Promega), and 10–100 ng μL^{-1} DNA.

The amplification was performed using an Eppendorf Mastercycler® gradient thermocycler (Eppendorf, Hamburg, Germany), with the amplification condition as follows: Initial denaturation for 4 min at 94

°C, followed by 35 cycles of 35 s denaturation at 94 °C, annealing at 55.5 °C for 30 s (18SAlexF1–18SAlexR1)/ 52.5 °C for 30 s (18SAlexF2–18SAlexR2)/ 55 °C for 50 s (D1R–D3Ca)/ 55 °C for 45 s (AlexITSf1–AlexITSr1), extension at 72 °C for 35 s (18SAlexF–18SAlexR, D1R–D3Ca)/ 1.5 min (AlexITSf1–AlexITSr1), and a final extension of 7 min at 72 °C.

Amplicons were purified with the Promega Wizard® PCR Preps DNA Purification System prior to sequencing. DNA sequencing was performed by Sanger sequencing on both strands using an ABI 3730XL DNA Analyzer (PE Biosystems, Vernon Hills, IL, USA).

2.3.2. Sequence analysis and phylogenetic reconstructions

Newly obtained sequences of the SSU, LSU, and ITS rDNA and related sequences retrieved from the NCBI GenBank nucleotide database (Table 1, Table S1) were multiple-aligned using Multiple Sequence Comparison by Log-Expectation, MUSCLE (Edgar, 2004).

Phylogenetic analyses of maximum parsimony (MP) and maximum likelihood (ML) were performed using PAUP* ver. 4.0b.10 (Swofford, 2001). MP was performed using heuristic searches with 1000 random-addition replications and branch-swapping with tree bisection and reconnection (TBR). Bootstrap analysis was performed with 1000 bootstrap replicates and 100 random additions of sequences run per bootstrap replicates. ML was performed using the best-fit model calculated by the Akaike information criterion in jModelTest 2.1.3 (Darriba and Posada, 2014), with 1000 random addition replications; heuristic searches were carried out with branch-swapping and TBR. Bayesian analysis (BI) was performed using MrBayes 3.2.2 (Ronquist et al., 2012), based on the same best-fit model, a four-chain run for 10^7 generations was used and trees were sampled every 100 generations; posterior probabilities (PP) were estimated with 20,000 generations burn-in.

All the SSU, LSU, and ITS rDNA datasets were used to calculate the sequence divergences of closely related species based on uncorrected pairwise p-distances using MEGA11.

2.3.3. ITS2 transcript modeling and CBC analysis

The nucleotide sequences of the ITS1–5.8S-ITS2 region obtained in this study and those retrieved from the GenBank (Table 1, Table S1) were used to identify the ITS2 region by annotating the 5.8S–LSU rRNA interaction (Keller et al., 2009). The ITS2 sequences were then used to model the secondary structures of ITS2 RNA transcript by homology modeling using the ITS2 Database V web interface (Ankenbrand et al., 2015) as outlined in Teng et al. (2016).

Orthologous alignment was guided by secondary structures of the ITS2 RNA transcripts using 4SALE v1.5 sequences-structure alignment (Seibel et al., 2008). A sequences-structure informative phylogenetic tree of ITS2 RNA transcript was reconstructed using ProfDistS v0.9.9 (Qt version) (Wolf et al., 2008) by neighbor-joining (NJ) using general time reversible (GTR) evolutionary model, followed by 1000 bootstrap replications. ML analysis was performed using Phargorn (Schliep, 2011) in R, with nonparametric bootstrap analysis (100 bootstrap replications and NNI optimization).

The ITS2 universal motifs of *Alexandrium* ITS2 transcripts were annotated based on previous studies (Coleman, 2009; Keller et al., 2009). The structures were illustrated using VARNA (Darty et al., 2009). Compensatory base changes (CBCs) and hemi-CBCs (HCBCs) were identified and mapped on the core ITS2 transcript (Teng et al., 2014). A CBC matrix table based on pairwise comparison was constructed by 4SALE.

2.4. Toxin analysis

2.4.1. Toxin extraction

For toxin analyses, strains were grown in 250 mL plastic culture flasks with the culture conditions described above. Cell densities from cultures in the early stationary phase (ranging from approximately 1×10^3 to 6×10^3 cells mL^{-1}) were determined by settling Lugol's iodine-fixed samples and counting >400 cells under an inverted microscope. Cells were harvested by centrifugation of multiple 50 mL subsamples (Eppendorf 5810R, 3220 × *g*, 10 min). The different cell pellets of one strain were resuspended, and combined in one microtube, centrifuged again (Eppendorf 5415, 16,000 × *g*, 5 min), and stored frozen (−20 °C) until use. For all strains, one cell pellet each was collected for analyses of lipophilic toxins and for PSP toxins (PSTs). Lipophilic toxins of strain Atay99Shio-02 were determined for three different cell pellets obtained from three independently grown cultures. The total number of cells harvested for these strains and the corresponding detection limits of toxins are listed in Tables S2 and S3. Note that the toxin profile of *A. pseudogonyaulax* strains could not be determined because both strains died off in the course of this study.

Cell pellets were extracted with 300 μL 0.03 M acetic acid for PST extraction and with 300 μL methanol for the extraction of lipophilic toxins and lyzing Matrix D (Thermo Savant) in a homogenizer (MagnaLyzer, Roche Diagnostics, Mannheim, Germany) for 45 s at 5500 m s^{-1}. The homogenates were centrifuged for 5 min at 13,200 × *g*. The supernatants were transferred to spin filters (0.45 μm, UltraFree, Millipore, Eschborn, Germany) and centrifuged for 30 s at 5700 × *g*. The filtrates were transferred to HPLC vials and stored at −20 °C until analysis.

2.4.2. Analysis of paralytic shellfish toxins

PST analysis was performed by two independent methodological approaches: ion-pair chromatography coupled to post-column derivatization and fluorescence detection (PCOX) and hydrophilic interaction liquid chromatography coupled to tandem mass spectrometry (HILIC-MS/MS).

The PCOX analysis was performed on a liquid chromatography system (LC1100 consisting of a G1379A degasser, a G1311A quaternary pump, a G1229A autosampler, and a G1321A fluorescence detector, Agilent Technologies, Waldbronn, Germany), equipped with a Phenomenex Luna C18 reversed-phase column (250 mm × 4.6 mm id, 5 μm pore size) (Phenomenex, Aschaffenburg, Germany) with a Phenomenex SecuriGuard precolumn. The column was coupled to a PCX 2500 post-column derivatization system (Pickering Laboratories, Mountain View, CA, USA). Eluent A contained 6 mM octane-sulfonic acid, 6 mM heptane-sulfonic acid, 40 mM ammonium phosphate, adjusted to pH 6.95 with dilute phosphoric acid, and 0.75% tetrahydrofuran. Eluent B contained 13 mM octane-sulfonic acid, 50 mM phosphoric acid, adjusted to pH 6.9 with ammonium hydroxide, 15% acetonitrile, and 1.5% tetrahydrofuran. The flow rate was 1 mL min^{-1} with the following gradient: 0–5 min isocratic A, 15–16 min switch to B, 16–35 min isocratic B, 35–36 min switch to A, 36–45 min isocratic A. The injection volume was 20 μL and the autosampler was cooled to 4 °C. The eluate from the column was oxidized with 10 mM periodic acid in 555 mM ammonium hydroxide before entering the 50 °C reaction coil, after which it was acidified with 0.75 M nitric acid. Both the oxidizing and acidifying reagents entered the system at a rate of 0.4 mL min^{-1}. The toxins were detected by dual-monochromator fluorescence (lex 333 nm; lem 395 nm). The data were processed with Chemstation software (Agilent, Santa Clara, CA, USA) and calibrated against external standards.

The HILIC-MS/MS was performed on an Acquity UPLC Glycan BEH Amide column (130 Å, 150 mm × 2.1 mm, 1.7 μm, Waters, Eschborn, Germany) equipped with an in-line 0.2 μm Acquity filter and thermostated at 60 °C with an isocratic elution to 5 min with 98% eluent B followed by a linear gradient of 2.5 min to 50% B and 1.5 min isocratic elution. The flow rate was 0.4 mL min^{-1}, and the injection volume was 2 μL. Mobile phase A consisted of water with 0.15% formic acid and 0.6% ammonia (25%). Mobile phase B consisted of water/acetonitrile (3:7, v/v) with 0.1% formic acid. Mass spectrometric experiments were performed in the selected reaction monitoring (SRM) mode on a Xevo TQ-XS triple quadrupole mass spectrometer equipped with a Z-Spray source (Waters, Halethorpe, MD, USA). Instrument parameters are given in Table S4 and used mass transitions in Table S5. PSTs were quantified by

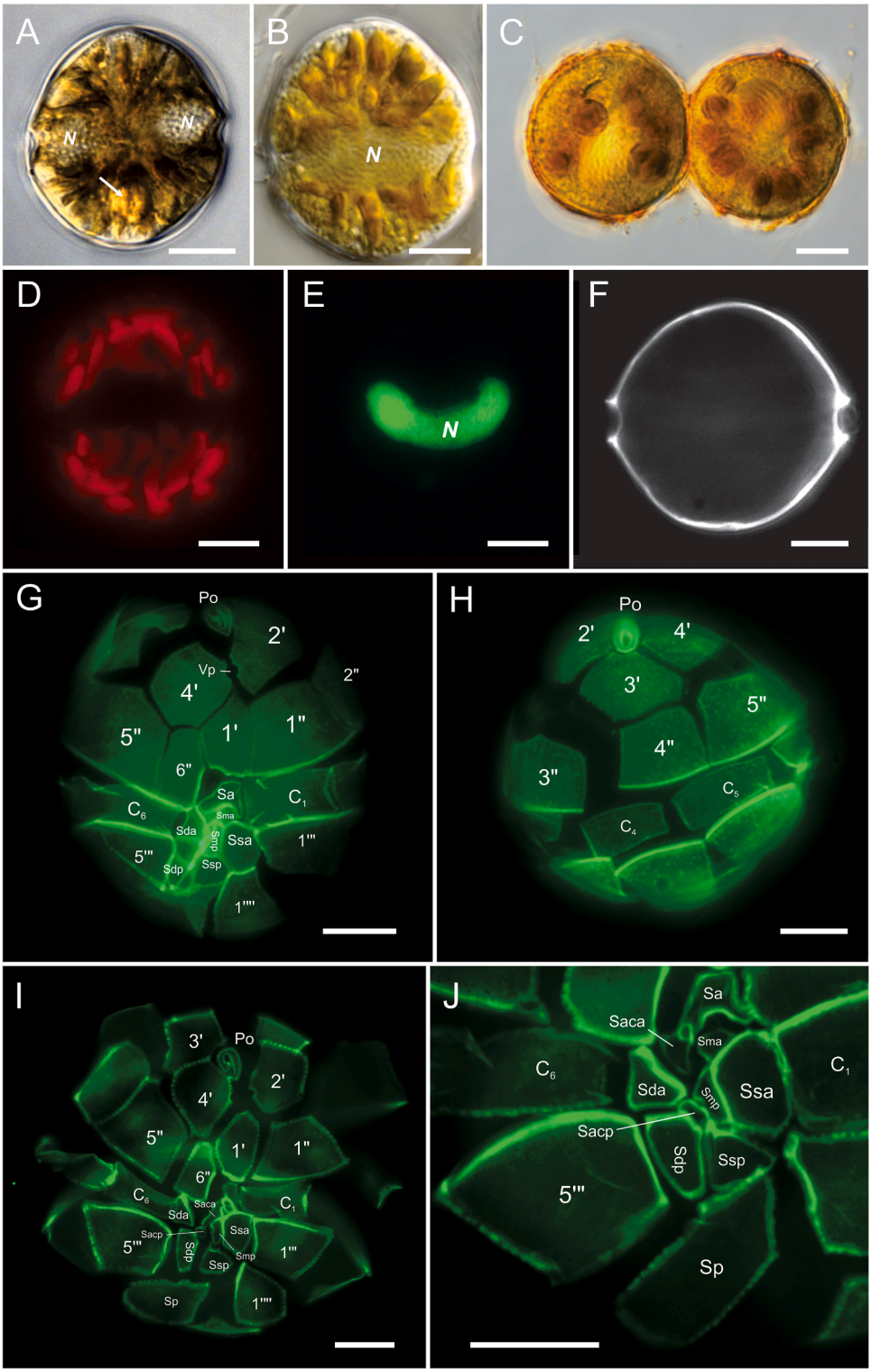

Fig. 1. *Alexandrium limii* sp. nov. (Strain DBS08). LM. (A–F) Live cells. (A–B) General size and shape from ventral-dorsal views. *N*, nucleus. Note the rounded structure (arrow in A), presumably a pyrenoid. (C) Newly divided pair of cells. (D–E) Different epifluorescence illumination of the same cell showing chloroplast distribution (D) and the shape and position of the SYTOX-Green stained nucleus (E) under blue light excitation. (F–J) Thecae of Solophenyl Flavine-stained cells. (F) Cell outline. (G) Cell in ventral and (H) dorsal view. (I–J) Details of sulcal plates. Sulcal plate labels: Sa, anterior sulcal; Ssa, left anterior sulcal; Ssp, left posterior sulcal; Sda, right anterior sulcal; Sdp, right posterior sulcal; Sma, anterior median sulcal; Smp, posterior median sulcal. Sp, posterior sulcal; Saca, anterior accessory; Sacp, posterior accessory. Scales, 10 μm.

external calibration with standard mix solutions of 4 concentration levels consisting of the following PSTs: STX, NEO, GTX2/3, GTX1/4, dcSTX, dcGTX2/3, B1, and C1/2. All individual standard solutions were purchased from the Certified Reference Materials Program (CRMP) of the Institute for Marine Biosciences, National Research Council (Halifax, Canada).

2.4.3. Analysis of lipophilic toxins

LC-MS/MS analysis for cycloimines was performed on a reversed-phase C18 column (Purospher STAR RP-18 end-capped (2 μm) Hibar HR 50–2.1, Merck, Darmstadt, Germany) equipped with a guard column (EXP Pre-column Filter Cartridge, Merck) and thermostated at 40 °C with an isocratic elution to 5 min with 5% eluent B followed by a linear gradient of 2.0 min to 100% B and 3.0 min isocratic elution prior to returning to initial conditions. The flow rate was 0.6 mL min^{-1}, and the injection volume was 0.5 μL. Mobile phase A consisted of 500 mL water with 955 μL formic acid and 75 μL 25% ammonia. Mobile phase B consisted of 475 mL acetonitrile, 25 mL deionized water, 955 μL formic acid and 75 μL 25% ammonia. Mass spectrometric experiments were performed in the selected reaction monitoring (SRM) mode in positive polarity on a Xevo TQ-XS triple quadrupole mass spectrometer equipped with a Z-Spray source (Waters). Instrument parameters are given in Table S6 and used mass transitions in Table S7. A standard solution of 100 pg μL^{-1} SPX 1 and 50 pg μL^{-1} GYM A (CRMP, IMB-NRC, Halifax, NS, Canada) were used for the determination of detection limits.

For the analysis of GDs, an alkaline elution system was used with eluent A consisting of aqueous 6.7 mM ammonia and eluent B of 6.7 mM ammonia in ACN/water (9/1 v/v). The flow rate was 0.6 mL min^{-1} and initial conditions of 20% B were held for 1.5 min. Then a linear gradient from 20% B to 90% B was performed within 2 min (until 3.5 min) followed by isocratic elution with 90% B for 0.5 min (until 4 min) prior to returning to initial conditions within 0.1 min and 0.9 min equilibration time (total run time: 5 min). The mass spectrometric parameters are given in Table S8, and the applied transitions are in Table S9. The collision energies for ammonium adducts were 30 eV and for sodium adducts 45 eV. Data were acquired and analyzed with MassLynx v.4.2 (Waters).

3. Results

3.1. Morphological characterization of Alexandrium species

Four morphotypes of *Alexandrium* were revealed from ten strains examined in this study (Table 1). Two morphotypes were identified as *A. pseudogonyaulax* and *A. taylorii* (two strains each) while two other morphotypes are proposed here to represent new species, *A. limii* sp. nov. and *A. ogatae* sp. nov., and the morphological descriptions of all species examined are presented below.

***Alexandrium limii* sp. nov.**

S.T.Teng, Tillmann, N.Abdullah, S.Nagai et Leaw

(Figs 1–5)

Description: Phototrophic, thecate dinophyte. Cells solitary or in short two-cell chains after division, spherical to subspherical in outline, 21–45 μm long, 21–46 μm wide. Thin theca with smooth surface and minute pores. Cingulum median, descending one cingular width, with cingular lists along anterior and posterior sutures. Thecal tabulation: Po, 4', 6", 6C, 8–10S, 5"', 2"". Plate 1' pentagonal, without contact with apical pore plate, left anterior margin shorter than right. Plate 6" longer than wide. Ventral pore usually located median on suture of 2' and 4'. Left anterior lateral sulcal plate (Ssa) large. Anterior sulcal plate (Sa) incised right posterior end of 1'. Sulcal lists present on right margin of plates 1"', 1"", and left margin of 5"'. Posterior sulcal plate (Sp) elongated, oblique to right.

Holotype: Glutaraldehyde-fixed material of strain DBS08 (labeled 'holotype of *Alexandrium limii*, prepared from strain DBS08, Batang Salak, Sarawak, 15/3/2017′) deposited at the Aquatic Botany Culture Collection, University Malaysia Sarawak, Malaysia.

Type locality: Batang Salak (1° 36′ 31.4886″ N, 110° 19′ 36.6774″ E), Sarawak, Malaysia Borneo.

Etymology: The species is named in honor of Dr. Po Teen Lim (Malaysia) for his contribution to the HABs research, development, and capacity building in Malaysia.

Additional specimens examined: strain Atay99Shio-02 from Shioya Bay (Japan) (Table 1, Figs 2–3).

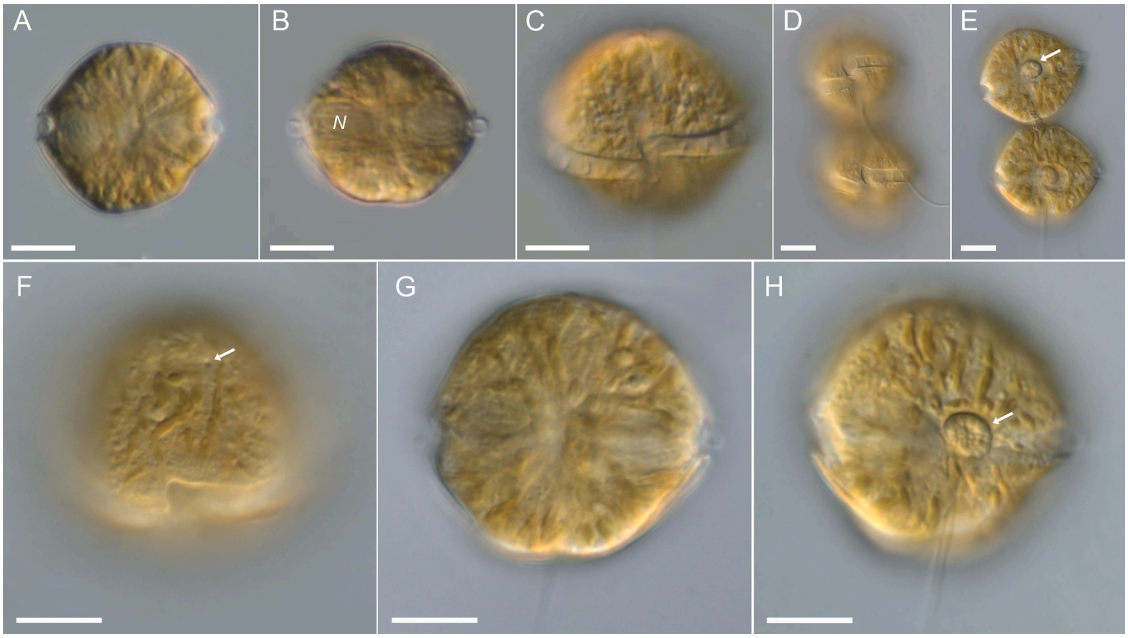

Fig. 2. *Alexandrium limii* sp. nov. (Strain Atay99Shio-02). LM. Live cells. General size and shape from ventral-dorsal (A–E, G, H), and ventral-apical (F) views. *N*, nucleus. (D, E) Newly divided pair of cells. Note the ventral pore (arrow in F) and a central rounded structure (arrows in E and H), presumably a pyrenoid. Scales, 10μm.

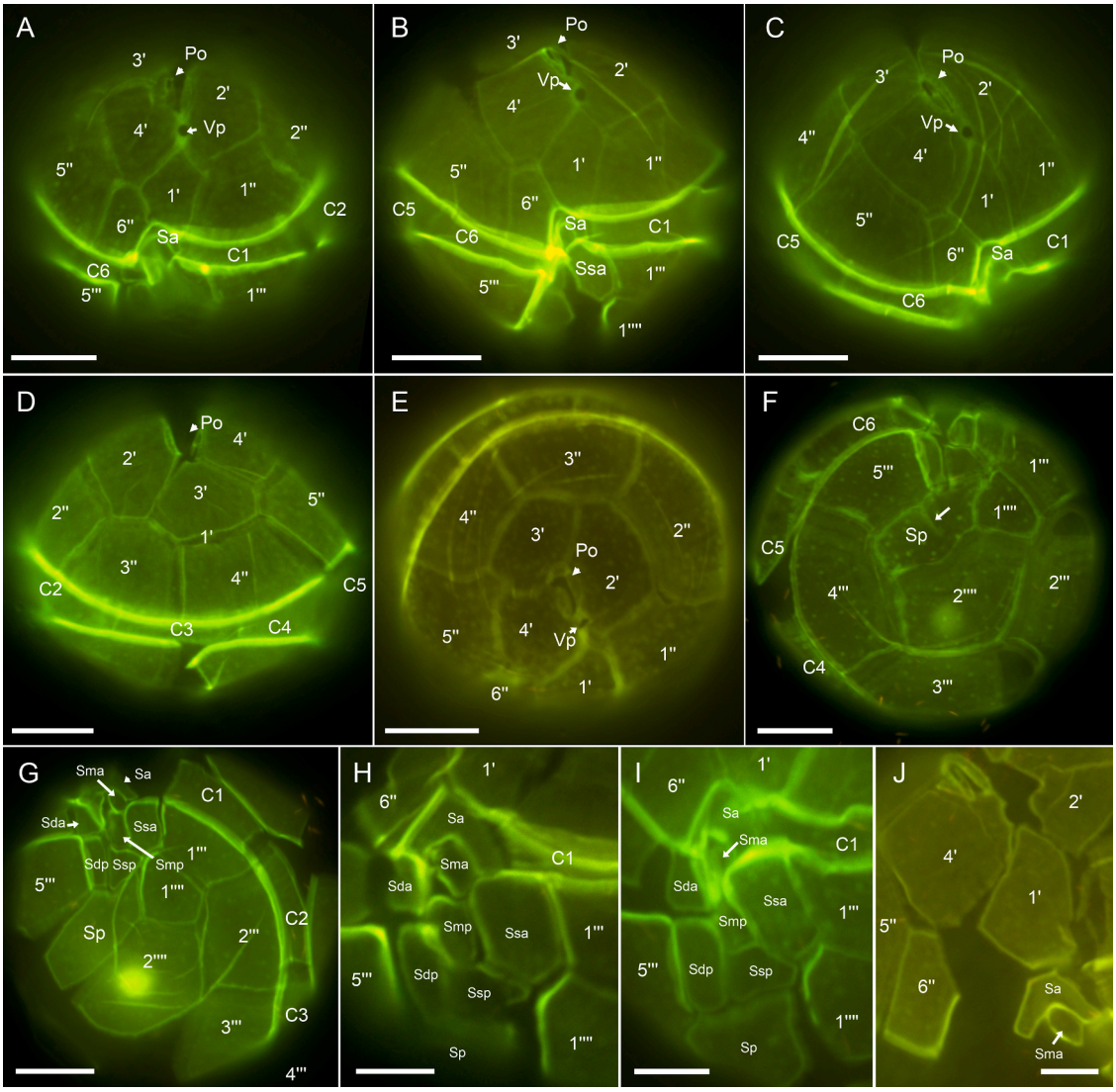

Fig. 3. . *Alexandrium limii* sp. nov. (Strain Atay99Shio-02). LM. Thecae of Solophenyl Flavine-stained cells under epifluorescence illumination. (A–C) Cells in ventral or ventral-apical, (D) dorsal, (E) apical, and (F–G) antapical views. Note the line or groove on plate Sp (arrow in F). (H–I) Details of sulcal plates. Sulcal plate labels: Sa, anterior sulcal; Ssa, left anterior sulcal; Ssp, left posterior sulcal; Sda, right anterior sulcal; Sdp, right posterior sulcal; Sma, anterior median sulcal; Smp, posterior median sulcal. Sp, posterior sulcal. (J) Detailed view of the ventral part showing plates 1', 6", and Sa. Scales, 10μm (A–G), 5 μm (H–J).

Alexandrium limii morphology

Light and epi-fluorescence micrographs of strain DBS08 are presented in Fig. 1, and strain Atay99Shio-02 in Figs 2 and 3. Cells were spherical to subspherical in outline (Figs 1–2), solitary, or in two-cell chains (Figs 1C, 2D–E). Cells were brownish orange in color (Fig. 1A–C), with numerous granular and ellipsoidal chloroplasts radially distributed from the center (Figs 1D, 2A). A round structure (potentially a pyrenoid) was located centrally or in the hyposome (Figs 1A, 2E, H). The nucleus was located in the cingular plane (Figs 1A–B, 2A–B), with both ends visible in the ventral view under LM (Fig. 1A); when stained with SYBR, the nucleus appears in a hemi-toroidal shape in the apical view (Fig. 1E). Cell dimensions measured from the three strains were 21–45 μm long (30.4 ± 4.5 μm, n = 169) and 21–46 μm wide (31.7 ± 4.5 μm, n = 169), with a length: width ratio of 0.7–1.2 (0.96 ± 0.07; n = 169) (Fig. 11A). The episome and hyposome were almost equal in size. The cingulum was median, with a cingular width of 2.5–6.2 μm (4.7 ± 1.2 μm; n = 160). The descending cingulum was displaced by one cingular width (Fig. 2C, D, 4A). The narrow cingular lists were present along the anterior and posterior sutures (Figs 1–3).

Cells of strain DBS08 were further examined with SEM as presented in Fig. 4. The cell was covered with thin and smooth thecal plates scattered with minute pores visible in SEM (Fig. 4). Thecal plates formula was typical for *Alexandrium*: Po, 4', 6", 6C, 8–10S, 5'", 2''". The plate arrangement is schematically illustrated in Fig. 5. The epitheca consisted of four apical plates (4'), six precingular plates (6"), and an apical pore plate (Po) (Figs 1, 3, 4). The ventrally positioned first apical plate 1' was consistently disconnected from the Po. It was pentagonal with two anterior margins, the left margin touching 2' being shorter than the right margin adjoining 4' (Figs 1G, I, 3A–C, 4A–D). The plate was 4.8–13.7 μm long (9.6 ± 1.8 μm; n = 132) and 2.9–8.7 μm wide (6.2 ± 1.2 μm; n = 87), with the ratio of length: width of 1.3–3.1 (1.71 ± 0.28; n = 87) (Fig. 11A).

A large ventral pore (Vp), which was visible occasionally in LM (Fig. 2F), was usually not in contact with the first apical plate 1' and was located on the suture between plates 2' and 4', forming similar-sized circular indentations on the edges of the right posterior margin of 2' and left anterior margin of 4'. This arrangement (Figs 1G, I, 3D) was observed for 64% of cells of strain DBS08 (n = 64); and for 57% of cells of strain Atay99Shio-02 (n = 77); However, in many cases, the distance between the anterior tip of plate 1and the pore plate (i.e. the suture length of 2/4) was so short that the Vp was seen almost in contact with 1' (Figs 3C, 4A, C), which was the case for 36% and 43% of cells of strains

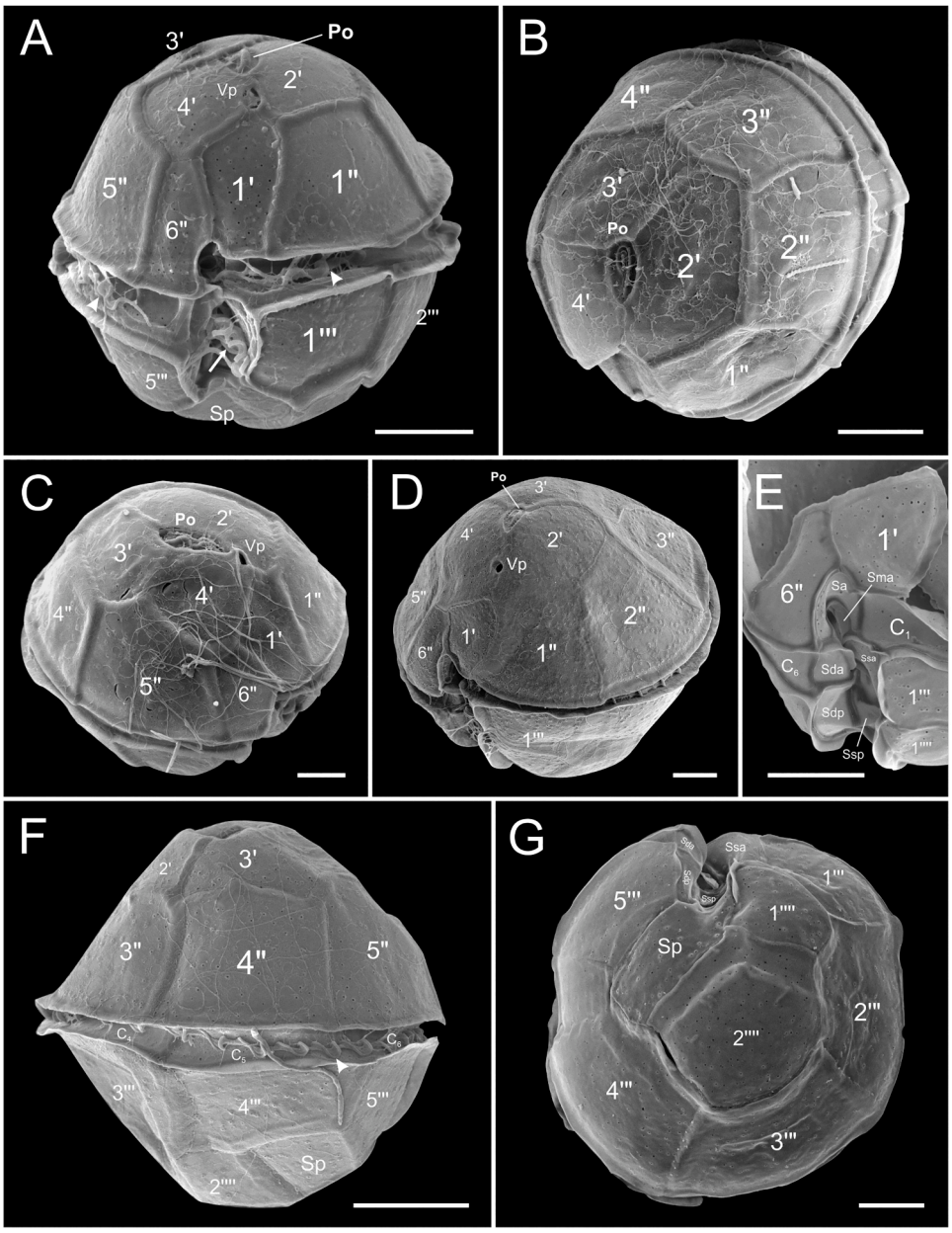

Fig. 4. *Alexandrium limii* sp. nov. (Strain DBS08). SEM. (A) Cell in ventral view. Note the longitudinal (white arrow) and transverse (white arrowhead) flagella. (B–D) Cells in apical view showing epithecal plates. (E) Detailed view of sulcal plates. Sulcal plate labels: Sa, anterior sulcal; Ssa, left anterior sulcal; Ssp, left posterior sulcal; Sda, right anterior sulcal; Sdp, right posterior sulcal; Sma, anterior median sulcal. Cells in (F) right-lateral view (F) and antapical view (G). Scales, 10μm.

DBS08 and Atay99 Shio-02, respectively. The length of sutures adjoined plates 2' and 4' (i.e., the distance between 1′and Po, herein referred 2'/4' suture) was 1.3–5.9 μm (3.5 ± 1.1 μm; $n = 74$), with the ratio of 2'/4' suture to 1' length ranging from 0.2 to 0.7 (0.4 ± 0.16; $n = 74$) (Fig. 11A). For cells with an unusual long suture of plates 2′and 4′, the Vp was consistently located almost exactly halfway between the anterior tip of 1′and the pore plate (Fig. 4D).

The Po was narrowly ovate, with a rounded dorsal and a pointed ventral end, and a hook-shaped pore was visible (Figs 1G–I, 3A–C, 4A–D). No anterior attachment pore was observed. The third apical plate 3' was symmetrical, positioned on the dorsal part of the epitheca (Figs 1H–I, 3D, E, 4B, C). Plate 6" was the smallest precingular plate, pentagonal, longer than wide (Figs 1G, I, 3A–C, J, 4A, C–E). The plate was 6.0–13.8 μm long (9.3 ± 1.4 μm; $n = 85$) and 3.2–7.8 μm wide (5.1 ± 0.9 μm; $n = 85$), with the ratio of length: width of 1.4–2.3 (1.86 ± 0.22; $n = 85$) (Fig. 11A).

The sulcus was narrow and short, bordered by sulcal lists on the right margin of the first postcingular plate (1''') and the first antapical plate (1''''), and the left margin of the fifth postcingular plate (5''') (Fig. 4A, E). The anterior sulcal plate (Sa) was narrow (Fig. 1G, J), situated almost perpendicularly below 1', and slightly invaded the epitheca (Fig. 4E). Its right lateral suture adjoined the left lateral margin of 6". Its anterior left lateral margin was a continuation of the right lateral margin of 1' (Fig. 4E). In the sulcus, the following eight larger plates were clearly identified: left anterior sulcal (Ssa), left posterior sulcal (Ssp), right posterior sulcal (Sdp), right anterior sulcal (Sda), anterior median sulcal (Sma), and the posterior median sulcal (Smp) plate (Figs 1G, I, J, 3G–I, 4E). Moreover, two small accessory sulcal plates, the anterior accessory (Saca) and posterior accessory (Sacp) plates were at times visible in fluorescence microscopy (Fig. 1I, J). The plate Ssa was the largest (Figs 1G, I, J, 3G–I), laid posteriorly to the Sa, with the anterior margin touching plate Sa, Sma, and C_1 (Figs 3H, I, 4E). The plate Sdp was

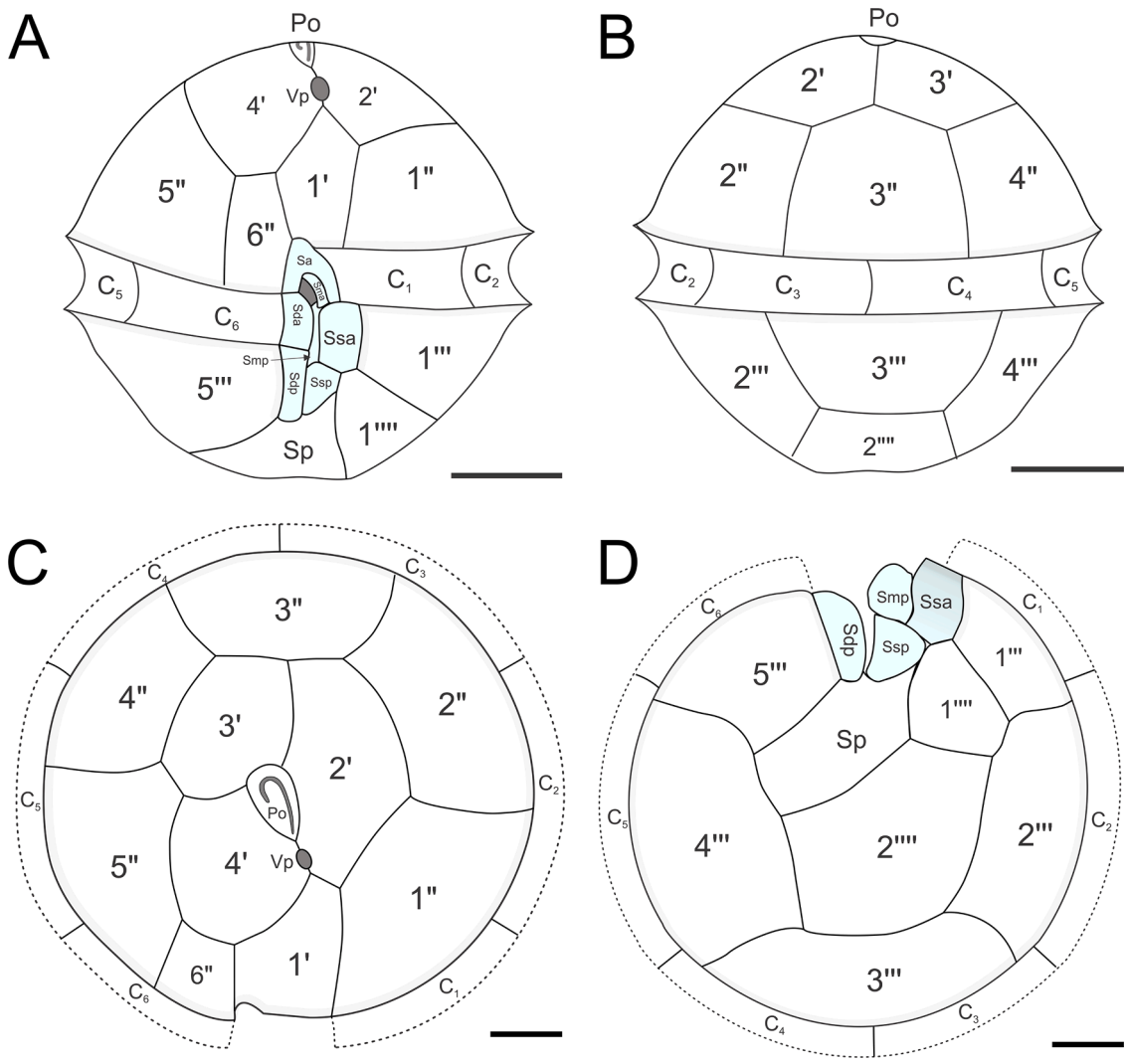

Fig. 5. Diagrammatic representation of thecal plate arrangement of *Alexandrium limii* sp. nov. (A) Ventral view. (B) Dorsal view. (C) Epithecal plates in apical view. (D) Hypothecal plates in antapical view. Scales, 10 μm.

slender and longer than the irregular triangular Ssp (Figs 1G, I, J, 3G–I, 4E). The plate Sda was triangular and had a small list covering the anterior and left margins of the plate (Figs 1G, I, J, 3H, 4E). Two small median sulcal plates, Sma and Smp, were identified (Figs 1I, J, 3G–I, 4E). The plate Sma was situated right below Sa (Fig. 1G, J, 3G–I) and vaulted over the flagellar pore (Fig. 4E). The plate Smp located between plates Ssa and Sdp was visible under epifluorescence microscopy (Fig. 1I, J, 3G–I), but this plate could not be demonstrated under SEM. Two accessory plates were at times observed; Saca was triangular, and Sacp was irregularly quadrangular (Fig. 1I, J). The Sp was elongated, longer than wide, and slanting to the posterior right (Figs 1J, 2F, G, 3 G). Occasionally a line or groove on plate Sp was present (Fig. 3F). The W-shaped anterior margin of the plate was in contact with the sulcal plates Sdp and Ssp (Figs 3F, G, I, 4 G). There were six cingular plates (C_1–C_6) of almost equal size (Figs 1G, H, 3D, F, G). The hypotheca comprised five postcingular plates, and two antapical plates. The first and fifth postcingular plates (1''' and 5''') were of comparable size and were the smallest among the postcingular plates (Figs 3F, G, 4 G). Plate 1'''' was trapezoidal, with a distinct sulcal list present on the right margin of the plate; the anterior margin touching Ssa, Ssp, and 1''' (Figs 1G, I, 3G–I, 4 G). The broad pentagonal plate 2'''' was located at the antapical position (Figs 3F, G, 4 G).

***Alexandrium ogatae* sp. nov.**

S.T.Teng, N.Abdullah, Tillmann, Leaw et P.T.Lim

(Figs 6–8)

Description: Photosynthetic, thecate dinophyte. Cells solitary, or in two-cell chains, subspherical to irregularly heptagonal in outline, 23–43 μm long, 25–48 μm wide. Rough theca surface with dense pores. Cingulum median, descending one cingular width, with cingular lists along anterior and posterior sutures. Thecal tabulation: Po, 4', 6", 6C, 8–10S, 5''', 2''''. Plate 1' pentagonal, no contact with apical pore plate, left anterior margin shorter than right. Plate 6" wider than long. Ventral pore absent. Small pore present on right anterior part of anterior sulcal plate (Sa). Sa incised right posterior end of 1'. Left anterior and posterior lateral sulcal plates (Ssa and Ssp) almost equal in size. Sulcal lists present on right margin of plates 1''', 1'''', Ssa, and left margin of 5'''. Posterior sulcal plate (Sp) elongated.

Holotype: Glutaraldehyde-fixed material of strain LASpbB10 (labelled 'holotype of *Alexandrium ogatae*, prepared from strain LASpbB10, Sepanggar Bay, Sabah, 15/3/2017') deposited at the Aquatic Botany Culture Collection, University Malaysia Sarawak, Malaysia.

Type locality: Sepanggar Bay (6° 5′ 29.3388″ N, 116° 7′ 39.2772″ E), Sabah, Malaysia Borneo.

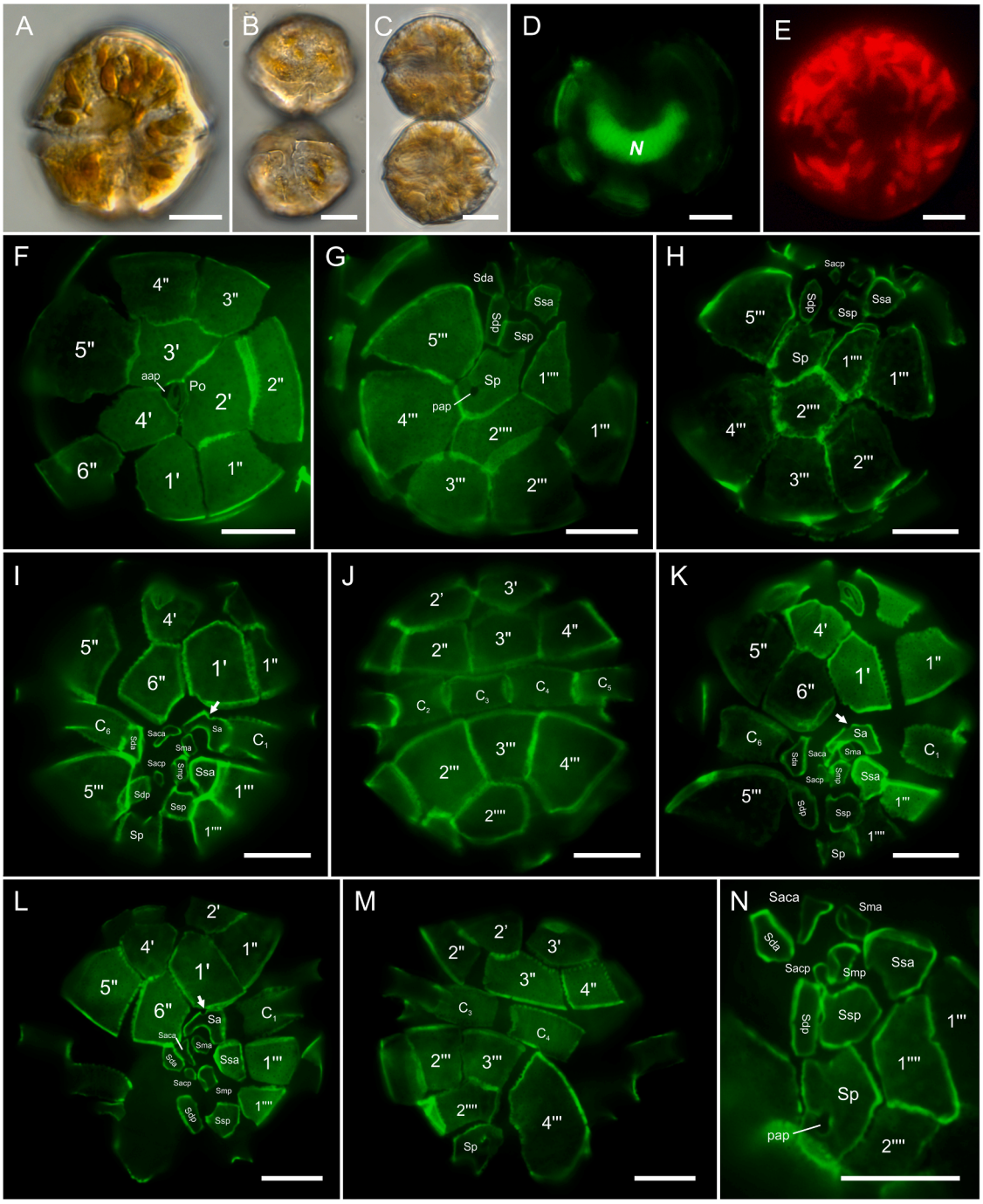

Fig. 6. *Alexandrium ogatae* sp. nov. (Strain LASpbB10). LM. (A–C) Live cells. (A) Subspherical cell. (B–C) Newly divided pair of cells. (D–E) Different epifluorescence illumination shows the shape and position of the SYTOX-Green stained nucleus, *N* (D), and chloroplast distribution under blue light excitation (E). (F–N) Thecae of Solophenyl Flavine-stained cells under epifluorescence illumination. (F) Apical view. (G–H) Antapical view. (I–J) Ventral view (I) and dorsal view (J) of the same cell. (K) Ventral view showing details of sulcal plates. (L–M) Ventral view (L) and dorsal view (M) of the same cell. (N) Details of sulcal plates. Note the presence of pore on the anterior sulcal plate (Sa) (white arrows). Sulcal plate labels: Sa, anterior sulcal; Ssa, left anterior sulcal; Ssp, left posterior sulcal; Sda, right anterior sulcal; Sdp, right posterior sulcal; Sma, anterior median sulcal; Smp, posterior median sulcal; Saca, anterior accessory; Sacp, posterior accessory. Scales, 10 μm.

Etymology: The species is named after Dr. Takehiko Ogata (Japan) for his contribution to the research in PSP toxins and capacity development in the Southeast Asian region.

***Alexandrium ogatae* morphology**

Cells of strains LASpbB10 and LASpbD3 were examined morphologically and the morphometrics was measured (Table 1), but only micrographs of strain LASpbB10 were presented (Figs 6, 7). Cells were solitary (Fig. 6A), or in two-cell chains (Figs 6B, C, 7C), with the cell outlines subspherical to irregularly heptagonal in ventral and dorsal views (Figs 6A–C, 7A–D). Cell content appeared brownish orange in color, with numerous ellipsoidal chloroplasts radially distributed from the center of the cell (Fig. 6A). The nucleus was located dorsally in the cingular plane (Fig. 6C); when stained with SYBR, the nucleus appeared hemi-toroidal shaped in the apical view (Fig. 6D). Cells were 23–43 μm long (32.6 ± 4.4 μm; $n = 107$) and 25–48 μm wide (32.5 ± 4.2 μm; $n = 107$), with a length: width ratio of 0.7–1.3 (1.01 ± 0.11; $n = 107$)

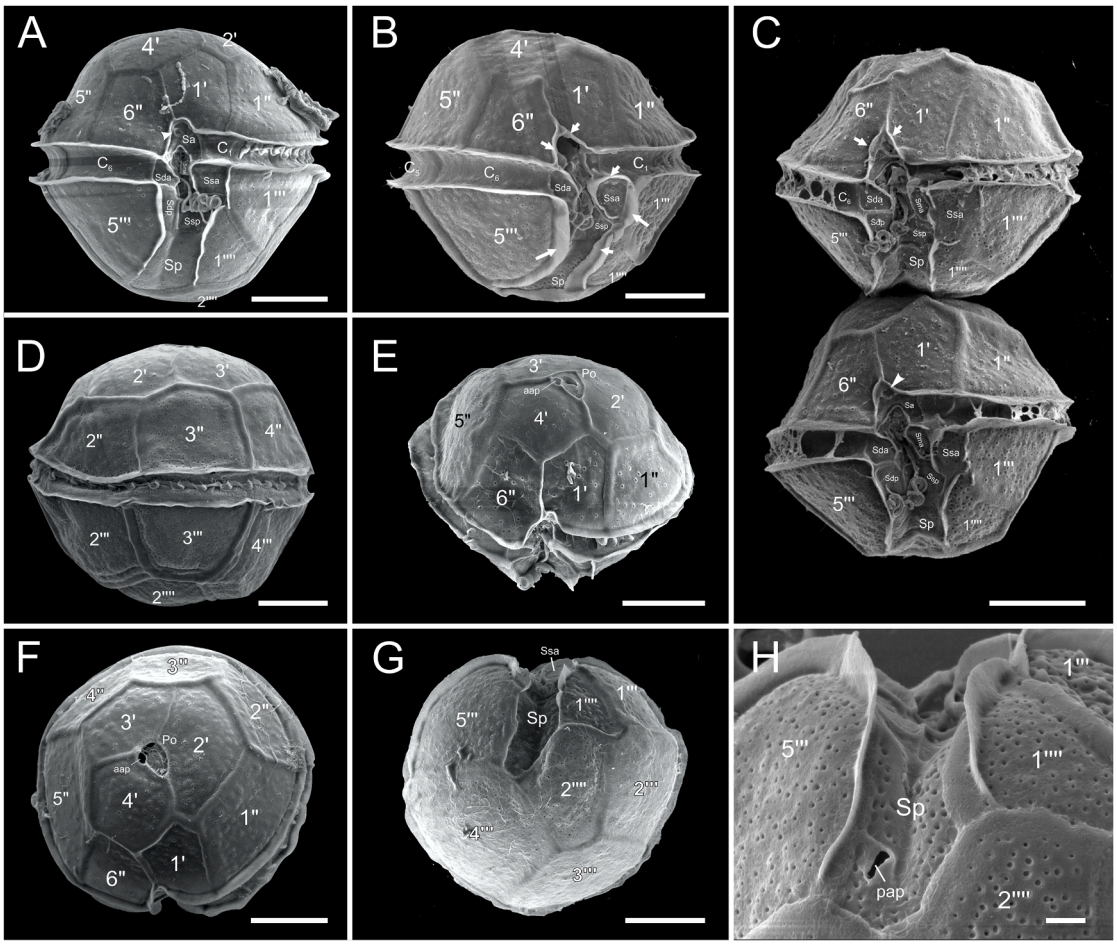

Fig. 7. *Alexandrium ogatae* sp. nov. (Strain LASpbB10). SEM. (A–C) Cells in ventral view. Note the pore on the anterior sulcal plate (Sa) (white arrowhead) (A, C) and the sulcal lists (white arrows) (B, C). (C) Cells in a two-cell chain. (D) Cell in dorsal view. (E–F) Cells in apical view. Note the presence of an anterior attachment pore (aap) at the left margin of Po. (G) Cell in antapical view. (H) Close-up of the posterior sulcal plate (Sp) showing the posterior attachment pore (pap). Scales, 10 μm (A–G), 2 μm (H).

(Fig. 11A). The episome was slightly shorter than hyposome. The cingulum was narrow and excavated, 3.9 ± 1.0 μm wide (2.3–6.3 μm; n = 160). The descending cingulum was displaced by one cingular width and covered with cingular lists along the anterior and posterior sutures (Fig. 7).

The cell was covered with thin thecal plates, rough with noticeable numerous pores scattered on the thecal plates (Fig. 7). Staining of thecal plates revealed the plate formula: Po, 4', 6", 6C, 8–10S, 5'", 2"". The plate arrangement is schematically illustrated in Fig. 8. The epitheca consisted of four apical plates, six precingular plates, and an apical pore plate (Po) (Figs 6–8). The ventrally positioned first apical plate 1' was consistently disconnected from the Po, pentagonal in shape, with the left margin touching 2' being shorter than the right margin adjoining 4' (Figs 6F, I, K, L, 7A–C, E, F). The length of plate 1' was 7.0–15.9 μm (10.7 ± 2.0 μm; n = 107), and the width of 4.0–11.8 μm (7.6 ± 1.6 μm; n = 61), with a ratio of length: width of 1.1–2.0 (1.44 ± 0.18; n = 61). There was no Vp in the specimens examined (n = 107). The length of the suture between plates 2' and 4' (herein referred 2'/4' suture) was 2.7–7.9 μm (4.9 ± 1.5 μm; n = 46), with the ratio of 2'/4' suture to 1' length ranging from 0.3 to 0.6 (0.46 ± 0.08; n = 46). The Po was ovate to irregularly triangular, with a slightly straight dorsal margin, and a hook-shaped pore was visible in the middle of the plate (Fig. 6F, K). In some cells, a large anterior attachment pore (aap) was seen located between the right margin of Po and 4' (Figs 6F, 7E, F). The apical plates 2', 3', and 4' surrounding the Po were almost equal in size; plates 3' and 4' were symmetrical. Plate 6" was pentagonal, usually longer than wide (Figs 6I, L, 7C). The plate was 5.6–12.4 μm long (8.7 ± 1.7 μm; n = 61) and 3.2–11.4 μm wide (6.9 ± 2.1 μm; n = 61), with the ratio of length: width of 0.9–2.3 (1.34 ± 0.39; n = 61) (Fig. 11A).

The sulcus was broad and shallow, slightly extending into the epitheca. It was bordered by sulcal lists on the right margins of the first postcingular (1'"), the first antapical (1""), the anterior sulcal plate (Ssa), and on the left margin of the fifth postcingular plate (5'"). In addition, there were short lists on the posterior margin of 1' and the left posterior margin of 6" (Fig. 7A–C). In the sulcal area, the left anterior sulcal (Ssa), left posterior sulcal (Ssp), right posterior sulcal (Sdp), right anterior sulcal (Sda), anterior median sulcal (Sma), and posterior median sulcal (Smp) plates(Figs 6I, K, L, N, 7A–C), and two accessory plates, anterior and posterior accessory (Saca, Sacp), were seen in fluorescence microscopy (Fig. 6I, K, L, N). Plate Ssa was located directly posterior to the first cingular plate (C_1) (Fig. 7A–C). The plate Sa was irregularly A-shaped. A pore was situated on the right anterior part of the plate (Figs 6I, K, L, 7A, C); when observed on the dissected plates, it appeared as a circular incise on the edge of the plate (Fig. 6I, K, L). Plate Ssp was comparable in size to Ssa, irregularly pentagonal in shape (Fig. 6G–I, K, L, N). Plate Sdp was elongated (Figs 6G, K, L, N, 7A, C). Plate Sda was triangular and had a small list covering the anterior and left margins of the plate (Figs 6G, I, K, L, N, 7A–C). Two small central median sulcal plates, Sma and Smp, were identified from fluorescence microscopy (Fig. 6I, K, L, N). The plate Sma was located next to the left posterior end of Sa and adjoined Ssa (Fig. 7A, C). Plate Smp and the two tiny accessory plates, Saca and Sacp, were observed in LM but not in SEM. The Saca was

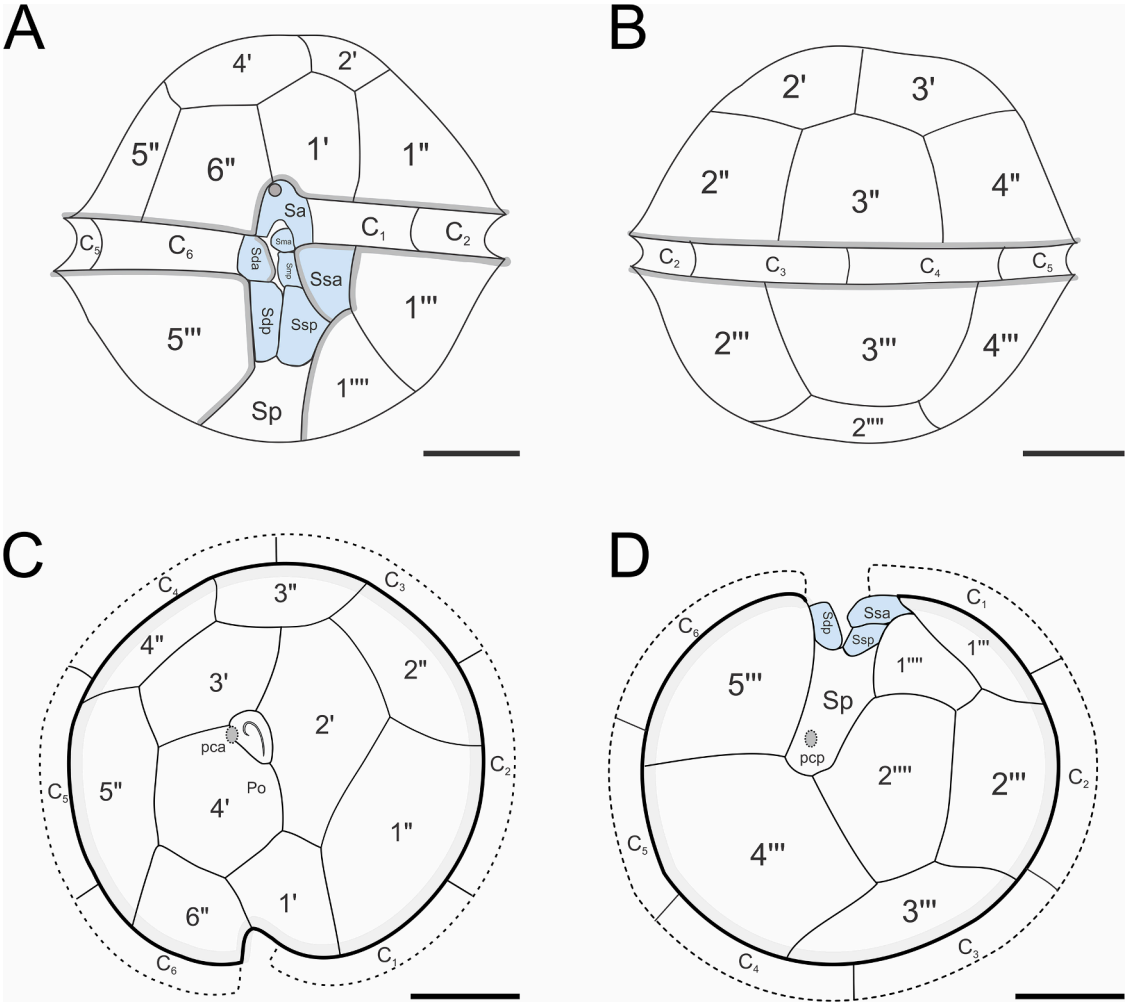

Fig. 8. Diagrammatic representation of thecal plate arrangement of *Alexandrium ogatae* sp. nov. (A) Ventral view. (B) Dorsal view. (C) Epithecal plates in apical view. (D) Hypothecal plates in antapical view. Scales, 10 μm.

long, oblique triangular, Sacp was the smallest sulcal plates (Fig. 6I, K, L, N).

The hypotheca comprised five postcingular plates and two antapical plates. Plate 4''' was the largest among the postcingular plates (Figs 6G, H, 7 G). Plate 1'''' was irregularly triangular, with a clear sulcal list present on the right suture of the plate (Figs 7G, H). The Sp was elongated, longer than wide, with an obliquely V-shaped anterior margin (Figs 6G, H, N, 7 G, H). In some cells, a relatively large irregular oval posterior attachment pore (pap) was observed on the right side of Sp (Figs 6G, M, N, 7H). Plate 2'''' was pentagonal, slightly longer than wide (Figs 6G, H, 7 G), located at the antapex, and positioned obliquely to the left ventral side of the cell (Fig. 7A, G).

***Alexandrium pseudogonyaulax* morphology**

Cells of *A. pseudogonyaulax* strains LMIAE9 and LATAG8 were subspherical and ranged from 21 to 42 μm in length (31.2 ± 4.8 μm; $n = 66$) and 24–45 μm in width (33.3 ± 5.0 μm; $n = 66$) in size. The length: width ratio of 0.8–1.4 (0.94 ± 0.09; $n = 66$) (Fig. 11A) was quite variable with some cells being longer than wide (Fig. 9A–C) or wider than long (Fig. 9I). The nucleus was located in the cingular plane, with both ends visible in the ventral view under LM (Fig. 9A–C); when stained with SYBR, the nucleus appears hemi-toroidal shaped in the apical view (Fig. 9D). The cells were brownish orange in color, with numerous granular chloroplasts visible under light (Fig. 9A–C) and fluorescence microscopy (Fig. 9E). The cingulum was narrow, displaced by approximately one cingular width (Fig. 9I).

The theca was composed of thin and smooth plates. Thecal plates were with typical *Alexandrium* plate tabulation: Po, 4', 6", 6C, 8–10S, 5''', 2'''' (Fig. 9F–K). Plate 1' was pentagonal, disconnected from Po, with a shorter left anterior margin (Fig. 9F, I, J). Occasionally, cells with a quadrangular 1' plate were observed (Fig. 9G). Plate 1' was 5.4–12.9 μm long (9.5 ± 1.8 μm; $n = 62$) and 4.0–9.5 μm wide (7.0 ± 1.3 μm; $n = 40$), with the length: width ratio ranging from 1.2 to 1.7 (1.43 ± 0.13; $n = 40$). The Po was surrounded by plates 2', 3', and 4'. A large ventral pore (Vp) was observed in the midpoint of the suture between 1' and 4' (Fig. 9F–G, I, J). The 2'/4' suture length was 3.0–7.8 μm (4.7 ± 1.2 μm; $n = 22$); the ratio of 2'/4' suture: 1' length was 0.4–0.7 (0.53 ± 0.07; $n = 22$). Plate 6" was pentagonal, slightly longer than wide (Fig. 9F–G, I); 6.1–13.9 μm long (9.3 ± 1.7 μm; $n = 40$) and 3.9–10.6 μm wide (6.4 ± 1.4 μm; $n = 40$), with the length: width ratio of 1.2–1.9 (1.48 ± 0.18; $n = 40$) (Fig. 11A). Plate Ssa was large and wide (Fig. 9F, H). The accessory sulcal plates, Saca and Sacp, were observed (Fig. 9F, H). Plate Sp was elongated and oblique to the right (Fig. 9G, K). Plate 2'''' was wider than long (Fig. 9K).

***Alexandrium taylorii* morphology**

Cells of *A. taylorii* strains AY7T and AY1T from the Adriatic Sea agreed largely with the original species description in Balech (1994). The thecal examination of the strain AY7T was presented in detail in Tillmann et al. (2020), and AY1T is presented here in Fig. 10. Thecal plate morphometric measurements were made on both strains for comparison (Fig. 11A).

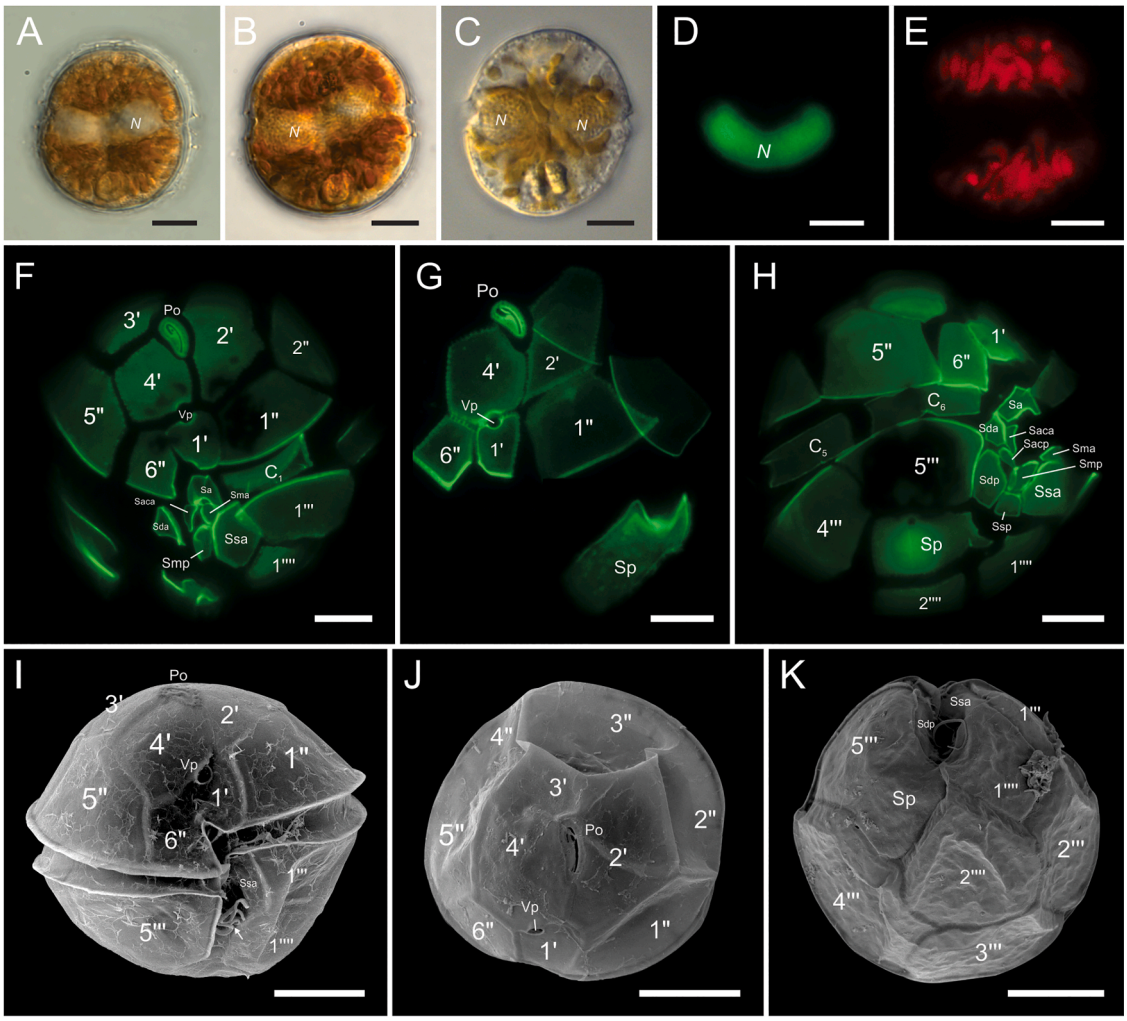

Fig. 9. *Alexandrium pseudogonyaulax* (Stain LATAG8). (A–H) LM. (A–C) Subspherical vegetative cells. *N*, nucleus. (D) Different epifluorescence illumination shows the shape and position of the SYTOX-Green stained nucleus, *N*, and (E) chloroplast distribution under blue light excitation. (F–H) Thecae of Solophenyl Flavine-stained cells under epifluorescence illumination. (F–G) Apical ventral view. Note the position of the ventral pore (Vp). (H) Detailed view of sulcal plates. Sulcal plate labels: Sa, anterior sulcal; Ssa, left anterior sulcal; Ssp, left posterior sulcal; Sda, right anterior sulcal; Sdp, right posterior sulcal; Sma, anterior median sulcal; Smp, posterior median sulcal; Saca, anterior accessory; Sacp, posterior accessory. (I–K) SEM. (I) Ventral view. The white arrow shows the longitudinal flagellum. (J) Apical view. (K) Antapical view. Scales, 10 μm.

Cells were solitary (Fig. 10A–D), but doublets were observed shortly after cell division (Fig. 10E). Cells were subspherical to irregularly hexagonal in outline (Fig. 10A–G) and 27–48 μm long (38.2 ± 4.6 μm; n = 102) and 27–49 μm wide (39.4 ± 4.9 μm; n = 102), with the length: width ratio of 0.9–1.1 (0.97 ± 0.04; n = 102). The cingulum was narrow and displaced by about one cingulum width (Fig. 10G, H). The plate tabulation was determined as Po, 4', 6", 6C, 8S, 5'", 2"" (Fig. 10H–O). Plate Po was disconnected from the pentagonal to quadrangular 1' (Fig. 10H–L, N–O). A large Vp was present above 1' and was located in the junction of plates 1', 2', and 4' (Fig. 10H–K, N). In the cultured material of strain AY1T there was some slight variability in the position of the Vp. In one out of 58 cells examined (2%), the Vp was located on the suture between plates 2' and 4' (not shown). Exceptional deviation in Vp position was also observed for the cultured cells of strain AY7T, where three of 75 examined cells (4%) had a Vp located on the suture of plates 2and 4' (see Supplementary Figure 1E, L, O in Tillmann et al., 2020). Moreover, for this strain, among the 75 cells examined in detail, one cell lacking an obvious Vp and one cell with two ventral pores (see Supplementary Figure 1S and 1T in Tillmann et al., 2020) were present. The length and width of 1' were 8.8–14.6 μm (11.0 ± 1.0 μm; n = 100) and 6.6–10.4 μm (8.5 ± 0.8 μm; n = 100), respectively; with the ratio of length: width of 1' ranging from 1.0 to 1.6 (1.31 ± 0.12; n = 100). The 2'/4' suture length was 4.8–12.0 μm (7.3 ± 1.3 μm; n = 85). The ratio of 2'/4' suture: 1' length was 0.5–0.9 (0.66 ± 0.09; n = 85). Plate 6' was irregularly pentagonal and longer than wide (Fig. 10H–O). Dimensions of plate 6' were 9.0–15.6 μm in length (10.8 ± 1.0 μm; n = 91) and 5.8–12.3 μm in width (7.5 ± 1.0 μm; n = 91), with a ratio of 6' length: width of 1.1–1.9 (1.46 ± 0.14; n = 91) (Fig. 11A).

In the sulcal area, plate Sa extended into the epitheca. This plate was narrow and not in contact with the first precingular plate (Fig. 10H, J). The posterior sulcal plate was elongated and at times had a conspicuous line or groove (Fig. 10O). The left sulcal plate was large (Fig. 10N, O) and the central sulcal area consisted of plates Sma, Smp, Ssp, Sda, and Sdp (Fig. 10O). Additional accessory sulcal plates were not observed.

3.2. Morphometric comparisons

The individual and variable plots of the morphometric data for the first (Dim1) and second (Dim2) principal components are shown in Fig. 11B. These first two dimensions express 91% of the total inertia; of which Dim1 accounts for 55% of the variation, while Dim2 for 36%. The total inertia was strongly greater than the reference value (22%), the variability explained by this plane is thus highly significant (Wilks test, $p < 0.0001$).

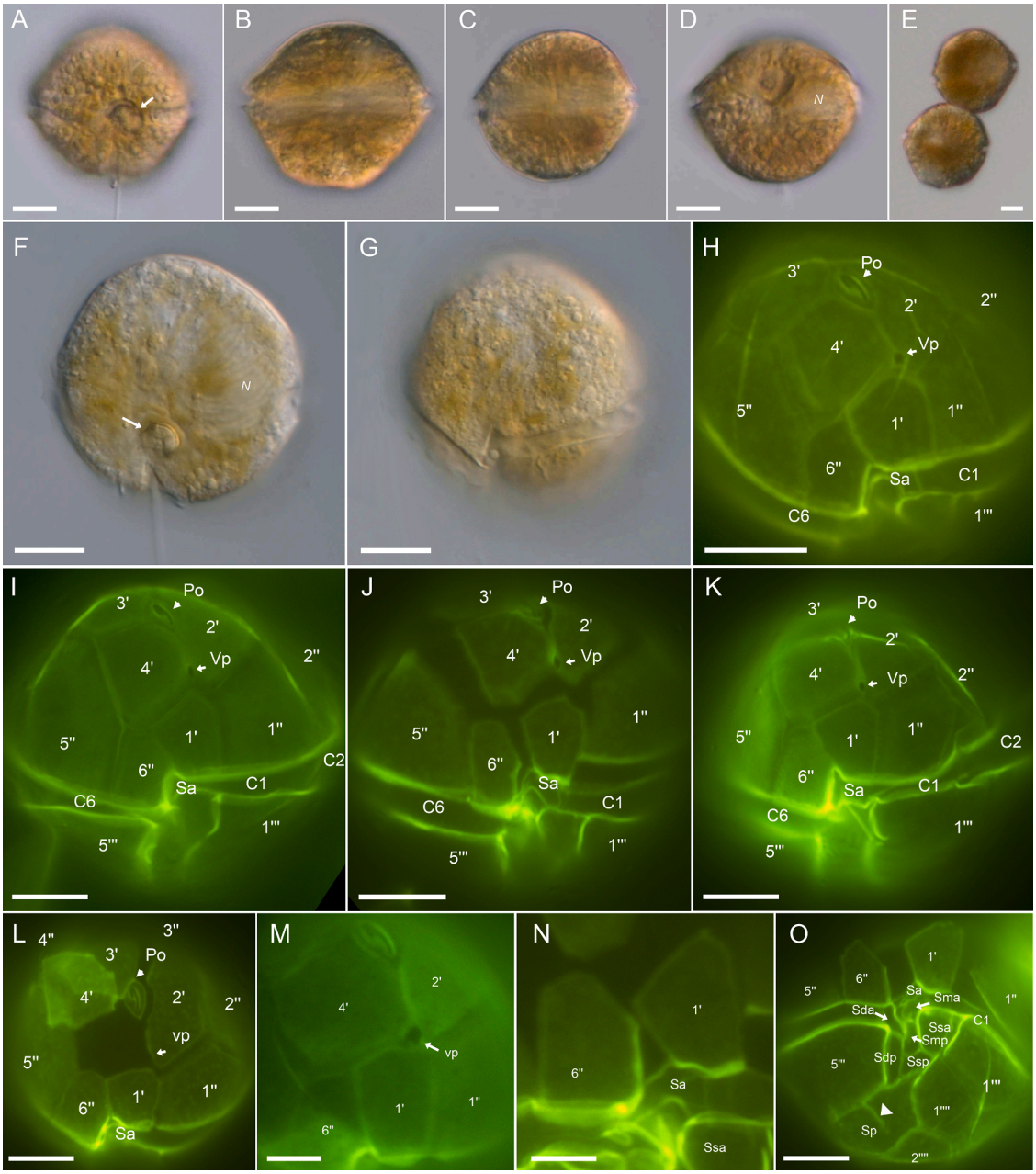

Fig. 10. *Alexandrium taylorii* (strain AY1T). LM. (A–G) Live cells. (A–E) General size and shape from ventral-dorsal view. (E) Newly divided pair of cells. (F, G) Two focal planes of the same cell in ventral-apical view. *N*, nucleus. Note the central rounded structure (arrows in A and F), presumably a pyrenoid. (H–O) Thecae of Solophenyl Flavine-stained cells under epifluorescence illumination. (H–L) Cells in ventral or ventral-apical view. (M, N) Detailed view of ventral epithecal plates. (O) Details of sulcal plates. Note the line or groove on plate Sp (arrowhead in O). Sulcal plate labels: Sa, anterior sulcal; Ssa, left anterior sulcal; Ssp, left posterior sulcal; Sda, right anterior sulcal; Sdp, right posterior sulcal; Sma, anterior median sulcal; Smp, posterior median sulcal; Sp, posterior sulcal. Scales, 10 μm (A–L, O) or 5 μm (M, N).

The first principal component (Dim1) has large positive associations with the ratio of 2'/4' suture:1' length, 2'/4' suture length, and width of 6", indicating informative descriptors of these traits. The dimension distributed cells of *A. taylorii* toward the positive values of Dim1, characterized by higher values for the ratio of 2'/4' suture:1' length, 2'/4' suture length, and the width of 6", separating them from other species. Whilst cells of *A. limii* were separated from *A. taylorii, A. ogatae*, and *A. pseudogonyaulax*, attributed to higher values for length: width ratio of 1', cell length: width ratio, and length: width ratio of 6" (Fig. 11B).

3.3. Molecular characterization

3.3.1. rDNA sequence information and phylogenetic inference

Nucleotide sequences of three nuclear-encoded rDNA (SSU, LSU D1-D3, and ITS) of *Alexandrium* species in this study were obtained to address species delineation. The newly obtained sequences of each *Alexandrium* strain and those retrieved from the GenBank nucleotide database are given in Table S1. Phylogenetic analyses of the three markers yielded identical tree topologies by MP, ML, and BI, with the BI trees shown for LSU, SSU, and ITS1–5.8S-ITS2 markers (Fig. 12, Figs S1–S3). While for the ITS2 sequence-structure tree reconstruction, the ML tree is presented (Fig. 12).

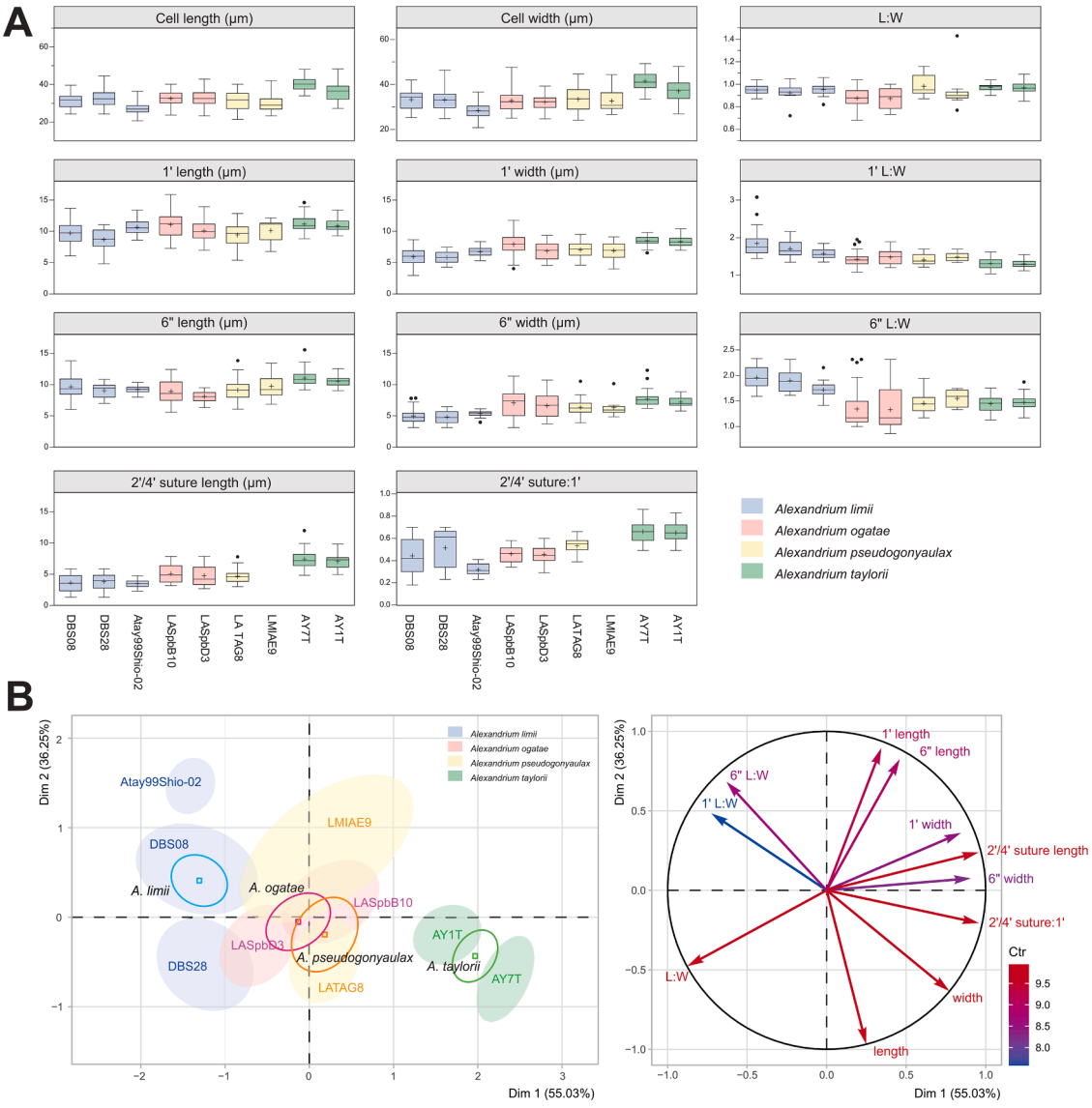

Fig. 11. (A) Box plots showing morphometric comparisons among strains of *Alexandrium limii* (DBS08, DBS28, Atay99Shio-02), *A. ogatae* (LASpbB10, LASpbD3), *A. pseudogonyaulax* (LaTAG8, LMIAE9), and *A. taylorii* (AY1T, AY7T). (B) Principal component analysis (PCA) ordination showing the multivariate variation among the strains with respect to the morphometric measurements, ellipses represent 95% confidence intervals for different strains (filled) and species (line). Vector directions indicate the morphometric traits' contribution to the first two dimensions.

The SSU rDNA multiple alignments of 112 taxa yielded 1655 characters, of which 656 were parsimony-informative, 78 were parsimony-uninformative, and 921 were constant. The LSU dataset of 108 taxa yielded a final alignment of 822 characters (555 were parsimony-informative, 57 were parsimony-uninformative, and 210 characters were constant). The ITS dataset yielded an alignment of 622 characters (549 were parsimony-informative, 12 were parsimony-uninformative, and 61 characters were constant). The phylogenetic reconstructions from these datasets are presented in Supplementary Figs S1–S3.

The trees showed a consistent monophyletic grouping of *A. limii, A. ogatae, A. taylorii*, and *A. pseudogonyaulax* (Fig. 12). In the LSU and ITS1–5.8S-ITS2 trees, *A. limii* formed a sister clade with *A. pseudogonyaulax*. In the SSU tree, it formed a sister clade with *A. taylorii. Alexandrium ogatae* consistently made up a basal node to *A. limii, A. taylorii*, and *A. pseudogonyaulax*, with strong nodal supports in both SSU and LSU trees (Fig. 12). In the ITS1–5.8S-ITS2 tree, it formed a sister clade to (*A. limii*+*A. pseudogonyaulax*). While the ITS2 sequence-structure tree revealed the sister relationship with *A. limii* (Fig. 12).

The pairwise sequence divergences (uncorrected *p*-distance) for *A. limii*, compared to its close relatives, ranged from 0.3 to 1.6% for the SSU dataset (Table S10), 4.2–13.4% for the LSU dataset (Table S11), and 23.2–24% for the ITS1–5.8S-ITS2 dataset (Table S12). While the pairwise uncorrected *p*-distances of *A. ogatae* to its close relatives ranged from 1.5 to 2% for the SSU dataset (Table S10), 12.3–13.9% for the LSU dataset (Table S11), and 15.3–18.5% for the ITS1–5.8S-ITS2 dataset (Table S12).

3.3.2. *ITS2 sequence-structure information*

The ITS2 secondary structures of *A. limii, A. ogatae, A. taylorii*, and *A. pseudogonyaulax* revealed the core features of the ITS2 transcript, with four common helices. Pairwise structural comparison of the ITS2 RNA transcripts between *A. limii* (Fig. 13A) and *A. ogatae* (Fig. 13B) revealed one CBC in Helix II (A-U↔G-C) and six HCBCs (Fig. 13C). When comparing with *A. pseudogonyaulax*, no CBC but six HCBCs were detected: two in Helix I (G-U↔G-C; U-A↔UG), one in Helix II (U-A↔U-G), two in Helix III (G-C↔G-U; U-G↔C-G) and one in Helix IV (U-G↔C-

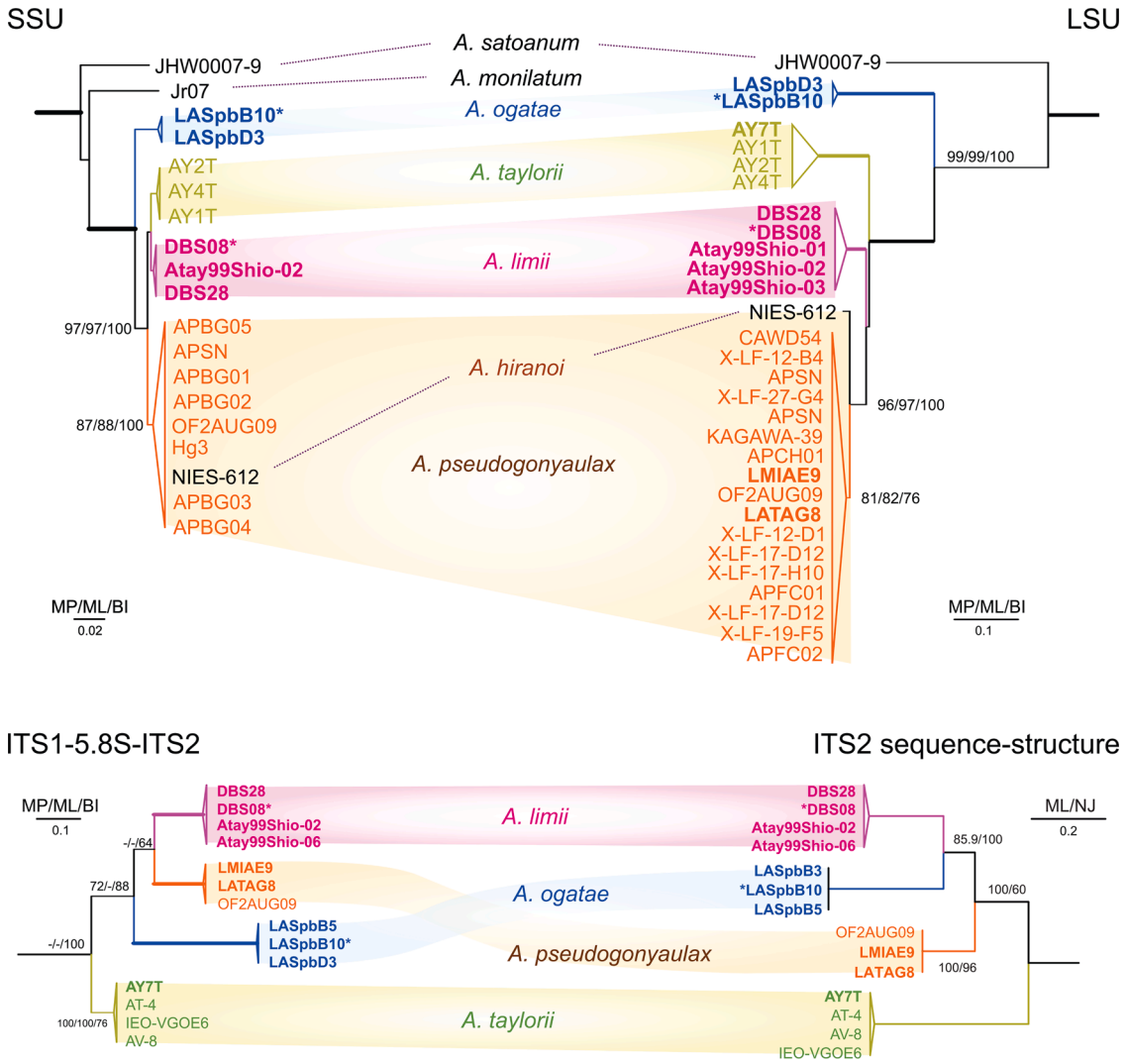

Fig. 12. Phylogenetic trees based on the SSU, LSU rDNA, ITS1–5.8S-ITS2, and ITS2 sequence-structure datasets of *Alexandrium* species. Nodal supports are bootstrap values of maximum parsimony (MP), maximum likelihood (ML), and Bayesian inference (BI), with only >50% supports shown. Nodal supports of 100% for all three analyses are marked with thick lines. See Supplementary Figs S1–S3 for detailed phylogenetic inferences.

G). The pairwise comparison of *A. limii* and *A. taylorii* revealed no CBC but three HCBCs: one in Helix I (G-U↔G-C) and two in Helix IV (G-U↔A-U; U-G↔C-G). The pairwise comparison of the ITS2 transcript of *A. ogatae* (Fig. 13B) with its close relatives showed two CBCs (in Helix III, A-U↔G-C; C-G↔U-A) and eight HCBCs for *A. pseudogonyaulax*; and five HCBCs for *A. taylorii* (Fig. 13C).

3.4. Toxin profiles

Two strains each of *A. taylorii, A. limii*, and *A. ogatae* (Table 2) were analyzed for toxins associated with the genus *Alexandrium*, namely PSTs, gymnodimines and spirolides (both belonging to the group of cyclo-imines), and goniodomins (GDs). None of the strains contained detectable levels of PSTs and cycloimines (for detection limits, see Tables S2, S3), but all strains contained GDs (Table 2). Both *A. taylorii* and *A. ogatae* strains contained GDA as major GD variants in the range between 6.3 and 13.7 pg cell^{-1}, and this was also true for the *A. limii* strain DBS08 isolated at the coast of Borneo, with a cell quota of 12.9 pg cell^{-1}. In contrast, the *A. limii* strain Atay99Shio-02 from Japan did not contain GDA, but a desmethyl variant of GDA. The cell quota of this putatively 34-desmethyl-GDA was determined on three independently grown subcultures and varied from 1.4 to 7.3 pg cell^{-1}. Also, *A. taylorii* strain AY1T contained a desmethyl variant of GDA as a minor component at a cell quota of 0.6 pg cell^{-1}, but clearly not the putative 34-desmethyl-GDA of *A. limii* strain AtayShio99–02. The collision-induced dissociation (CID) spectrum of this compound strongly suggests a 9-desmethyl configuration of GDA (data not shown). Detailed information on the structural characteristics of the GDA desmethyl variants will be reported elsewhere.

4. Discussion

4.1. Comparison of new species with their closely related species

Alexandrium limii is morphologically and genetically closer to *A. taylorii*, and this explains that some Pacific strains previously identified as *A. taylorii*, in fact, represent the new species *A. limii*. This refers to the Japanese strains (included in the present study) and the *A. taylorii* strain described by Lim et al. (2005), which we here also can reassign as *A. limii* after thorough morphological observations of the field specimens from the same location and comparison with clonal cultures. Both *A. taylorii* and *A. limii* share a longer-than-wide pentagonal plate 1' (Balech, 1995; Tillmann et al., 2020; this study), with the left posterior margin touching C_1 (Tillman et al., 2020). Nonetheless, both species are readily distinguishable by the plate and morphometric differences as examined in this study. *Alexandrium limii* is slightly smaller compared to

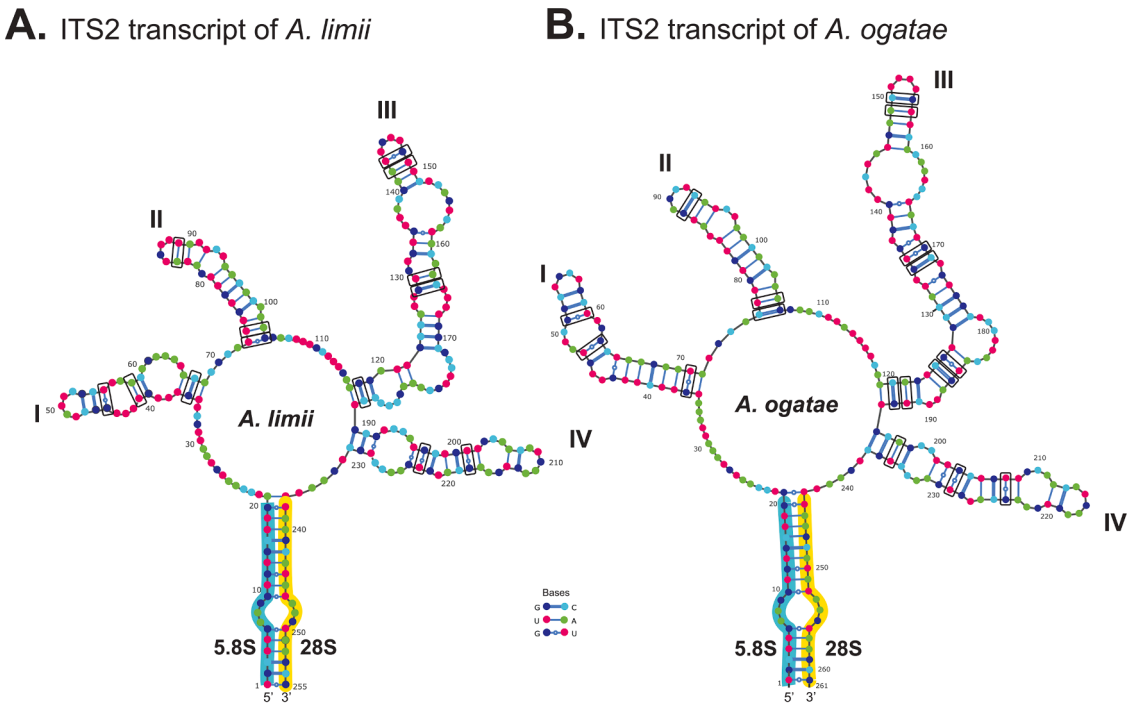

C. Pairwise comparison of CBCs (lower panel) and HCBCs (upper panel)

		a	b	c	d
A. pseudogonyaulax	*a*	0	8	6	2
A. ogatae	*b*	2	0	6	5
A. limii	*c*	0	1	0	3
A. taylorii	*d*	0	0	0	0

Fig. 13. ITS2 RNA transcripts of *A. limii* sp. nov. (A) and *A. ogatae* sp. nov. (B). The rectangles indicate the positions of compensatory base changes (CBCs) or hemi-CBCs (HCBCs) when compared to other closely related species, were observed. (C) Pairwise comparison of the number of CBCs (lower diagonal) and HCBCs (upper diagonal) among the closely related species.

A. taylorii. More importantly, the 2'/4' suture length in relation to the length of plate 1' is shorter in *A. limii* when compared to that of *A. taylorii*; and plates 1' and 6" are relatively narrower in *A. limii*, with larger length: width ratios (Fig. 11A). Morphometrics multivariate comparison by PCA further supported the separation of the two species (Fig. 11B). They are also distinguishable by the position of Vp. The Vp of *A. limii* is located on the suture between 2' and 4' forming circular indentations on the edges of the plates. However, when the suture length of 2' and 4' is short, this can be difficult to observe and the Vp is located very close to the junction of 1', 2' and 4'. The Vp of *A. taylorii* is usually located in the confluence point of either 1' and 4' or 1', 2', and 4' (Balech, 1995; Tillmann et al., 2020), although it must be noted that in the cultured material, rare exceptions of cells with a Vp disconnected from plate 1′and located on the 2′/4′suture were also observed. Complementary studies on the Vp position of field samples are needed to finally evaluate if such rare deviation of Vp position can be explained by culture artifacts. While the morphological trait of the presence/absence of Vp in *Alexandrium* has been regarded as taxonomic uninformative (Hansen et al., 2003) the presence/absence of Vp of the species examined in this study (disregarding the single cell of *A. taylorii* strain AY7T, for which no vp could be identified, see Suppl. Fig. 1S in Tillmann et al., 2020) was stable intra-specifically.

With its metasert plate 1' and lacking a Vp, *A. ogatae* is different from almost all other *Alexandrium*. The only similar species is *A. foedum* (Balech, 1990); which also lacks a Vp and has a small notch located on the right or middle part of the anterior margin of Sa. The species, however, differ from *A. foedum* originally described by Balech from the Gulf of Salerno, Italy (37–48.5 μm long, 40–53 μm wide; Balech, 1990) by having a smaller cell size range (23–43 μm long, 25–48 μm wide). Furthermore, the left and right lateral margins of 1' are almost parallel in *A. ogatae* (Fig. 7A–C, E), whereas they are non-parallel in *A. foedum* causing the posterior part of 1' to be narrow (Balech, 1990). Plate 3' of *A. ogatae* is symmetrical (Fig. 6G, 7F) but the plate is asymmetrical in *A. foedum* (Balech, 1990). The cingulum of *A. ogatae* is descending by about one cingular width but in *A. foedum* it is usually less than one cingular width (0.5–0.75; Balech, 1990). Genetically, *A. ogatae* singled out and formed a strong basal node to *A. limii, A. pseudogonyaulax*+*A. hiranoi*, and *A. taylorii* in the SSU and LSU trees (Fig. 12). However, no molecular data on *A. foedum* is currently available to assess if the two species are indeed the closest. It is noteworthy that Ssa of *A. ogatae* is particularly superficial (not inside the sulcus) and look as though a precingular than a sulcal plate.

The two new species readily differ from *A. pseudogonyaulax* by the position of Vp, where the Vp of *A. pseudogonyaulax* is consistently located on the suture between 1' and 4'. Cells of *A. pseudogonyaulax* examined in this study (Fig. 9) largely conform with the original description of *A. pseudogonyaulax* (Biecheler, 1952), with slight differences in the cell shape. *Alexandrium pseudogonyaulax* described by Biecheler (1952) is explicitly compressed (wider than long) (Balech, 1995). However, cells with both a compressed form and a slightly longer-than-wide cell shape were observed in this study. Also, cells of *A. pseudogonyaulax* from Danish waters were reported to exhibit large

Table 2
Toxins profiles and cell quotas of the investigated *Alexandrium* strains. For *A. limii* strain Atay99Shio-02, three different cell pellets obtained from three independently grown cultures have been analyzed for lipophilic toxins. nd, not detected. The number of cells analyzed for each species/strain/pellet and the limit of detection (LOD) for lipophilic toxins and for individual PST compounds are listed in Suppl. Tables S2–S3.

Species (strain)	lipophilic toxins Goniodomins [pg cell^{-1}]					Hydrophilic toxins
	GDA	34-desM-GDA	9-desM-GDA	SPX	GYM	PSTs
A. limii (DBS08)	**12.9**	nd	nd	nd	nd	nd
A. limii (Atay99Shio-02)	nd	**7.3**	nd	nd	nd	nd
A. limii (Atay99Shio-02)	nd	**1.4**	nd	nd	nd	nd
A. limii (Atay99Shio-02)	nd	**7.2**	nd	nd	nd	nd
A. ogatae (LASpbB10)	**13.7**	nd	nd	nd	nd	nd
A. ogatae (LASpbD3)	**6.3**	nd	nd	nd	nd	nd
A. taylorii (AY1T)	**6.8**	nd	**0.6**	nd	nd	nd
A. taylorii (AY7T*)	**11.7**	nd	nd	nd	nd	nd

* data from Tillmann et al. (2020)

variability in cell shape (Kremp et al., 2019). Nonetheless, these cell shape characters have been used to differentiate between *A. pseudogonyaulax* and *A. hiranoi*, where *A. hiranoi* is described with a longer-than-wide cell shape (Kita and Fukuyo, 1988; Balech, 1995). It is interesting to note that both species are genetically closer, this is supported by the sequence of *A. hiranoi* NIES-612 strain from the type locality (Jogashima Island, Japan) being recovered as a sister taxon in the LSU tree with strong nodal supports (Kim et al., 2005; Fig. S2). Cell shape is likely not a good diagnostic feature to distinguish between the two species, but according to the literature (Kita and Fukuyo, 1988; Balech, 1995) they are additionally differentiated by the position of Vp and the shape of 1′.

4.2. Species concepts in subgenus *Gessnerium*

The present study confirms previous phylogenetic studies indicating that the morphological concept of Balech (Balech, 1995), considering a metasert or exsert first apical plate (1') without clear contact to the pore plate (Po) as a synapomorphy of *Gessnerium*, a subgenus of *Alexandrium*, failed. Three of Balech's *Gessnerium* species, i.e., *A. insuetum, A. margalefii*, and *A. pohangense* in the present and many previous phylogenetic studies were unrelated to other *Gessnerium* species and grouped with species of the subgenus *Alexandrium sensu* Balech (Balech, 1995). While both *A. margalefii* and *A. pohangense* clustered next to each other in a well-supported clade with *A. leei, A. insuetum* is quite distantly embedded in the cluster of *A. minutum, A. tamutum*, and the allied species, and this again underlines the paraphyletic nature of a metarsert/exsert 1' plate. The question now arises if there are morphological features unifying all species of the molecularly defined *Gessnerium* clade. In a first attempt, a dichotomous identification scheme was constructed which enables species differentiation of those species of Balech's morphological *Gessnerium* concept (Fig. 14). By using morphometry of plate Sp, this tree indicates that the three "outlier" species (*A. insuetum, A. margalefii*, and *A. pohangense*) do not share the elongated and oblique Sp, which is typical for most species of the molecularly defined *Gessnerium* clade. The *Gessnerium* clade species *A. monilatum* and *A. satoanum* also do not have an elongated oblique Sp, but their Sp is broad and thus different from those of *A. insuetum* (Sp wider than long) and *A. margalefii/A. pohangense* (Sp longer than wide). The shape of the Sp plate of *A. globosum* is very similar to that of *A. margalefii* and *A. pohangense,* suggesting that this species probably is not included in the molecularly defined *Gessnerium* clade. The same likely refers to *A. concavum* and *A. camurascutulum*, whose Sp plate is similar in shape to the Sp of *A. insuetum*. Based on Fig. 14 it may be concluded that *A. balechii, A. foedum* (species of Balech's *Gessnerium*, but no molecular data available yet), with their elongated oblique Sp, are likely also

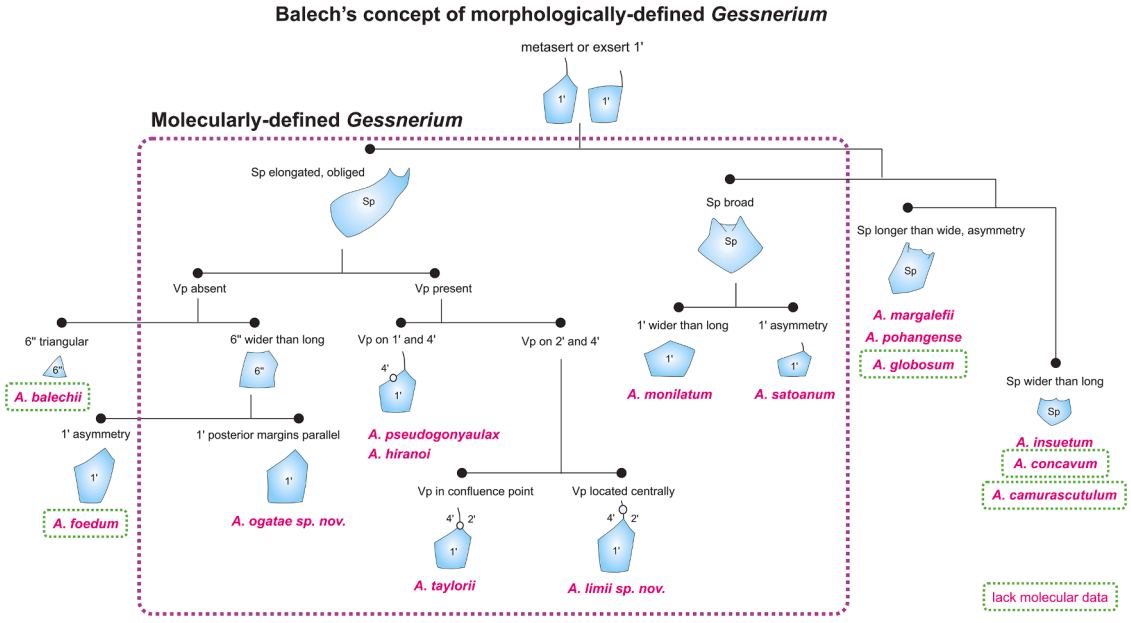

Fig. 14. A dichotomous diagram of diagnostic thecal features of *Alexandrium* species with metasert/exsert first apical plate (1'). Note that there is a Genbank LSU sequence AF032348.1 annotated as *A. concavum*, but this strain, based on morphology presented in MacKenzie et al. (2004), is *A. gaarderae* L.Nguyen-Ngoc & J. Larsen, a species with an elongated rhomboid 1′contacting the pore plate.

members of the molecularly defined *Gessnerium* clade. However, more efforts are needed to obtain sequence data of these up-to-now poorly known species of *Alexandrium* to clarify their phylogenetic position.

4.3. GD-producing Alexandrium species

With the description of *A. limii* and *A. ogatae* as new and GD-producing species, the number of GD-producing species of *Alexandrium* has increased to six, adding *A. limii* and *A. ogatae* to the already known GD producers *A. monilatum, A. hiranoi, A. pseudogonyaulax*, and *A. taylorii* (Tillmann et al., 2020). Thus, the production of GD seems to be a common trait, i.e. a chemical synapo"morphie" for all the species of the molecularly defined *Gessnerium* clade of *Alexandrium*. Only one of the species in this clade, *A. satoanum*, has not been tested yet for the presence of GD, likely because no cultured strains are currently available. Likewise, it would be interesting to grow and test other strains with a *Gessnerium*-type 1' configuration but of unknown phylogenetical position, i.e., *A. balechii, A. concavum, A. camurusculatum, A. foedum* and *A. globosum* for the presence of GD. In any case, almost all species and strains of the *Gessnerium* clade reported to date produce GDA as the major component of the GD profiles. The most notable exception by now is the Japanese *A. limii* strain Atay99Shio-02 which produced exclusively a desmethyl variant of GDA, most likely 34-desmethyl-GDA, at a cell quota comparable to GDA of the other strains. Desmethyl variants have been reported before in planktonic field samples of the Danish Limfjord and in 11 out of 17 clonal strains of *A. pseudogonyaulax* isolated from this area (Krock et al., 2018), erroneously reported as GDB (Harris et al., 2021). The same compound is reported here for *A. taylorii* strain AY1T from the Mediterranean (Table 2). However, the desmethyl variants of all these strains are putatively 9-desmethyl-GDA and were only produced as minor compounds besides GDA. Due to the low number of available GD-producing strains, it is still impossible to say, if these differences in GD profiles are associated with certain species and/or geographic patterns. It is interesting to note that all of the GD-producing strains do not produce PSTs (Krock et al., 2018; Tillmann et al., 2020; this study). However, one strain (reported as *A. taylorii*, reassigned here as *A. limii*) was reported to contain extremely low cellular contents of <1 fmole cell^{-1} by HPLC (Lim et al., 2005), which is in need of analytical confirmation by LC/MS-MS.

5. Conclusion

Two novel *Alexandrium* species were described based on both morphology and molecular evidence, hereby the names *Alexandrium limii* sp. nov. and *A. ogatae* sp. nov. were proposed. Both new species were shown to produce GDA, and this is the first report of the occurrence of GD-producing *Alexandrium* species in the Southeast Asian region. Although there is no evidence of human intoxication nor cases of GD contamination reported in the Western Pacific, GD analyses should be included in routine toxin monitoring and shellfish sanitation programs in the region as a proactive measure to safeguard human health and seafood safety.

Declaration of Competing Interest

The authors declare that they have no known competing financial interests or personal relationships that could have appeared to influence the work reported in this paper.

Data availability

Data have been shared as supplementary materials.

Acknowledgments

The work was supported by the Ministry of Higher Education, Malaysia, Higher Institution Centers of Excellence Grant [HICoE IOES-2023B] and Long-term Research Grant Scheme (LRGS) [LRGS/1/2020/UMT/01/1/3] to P.T. Lim; Universiti Malaysia Sarawak RISE award (UNI/F07/RISE/85756/2023) to S.T. Teng; and the PACES II research program of the Alfred-Wegener-Institute (AWI) as part of the Helmholtz Foundation initiative in Earth and Environment to U. Tillmann. Special thanks to Thomas Max and Anne Müller (both AWI Bremerhaven, Germany) for their continued support in toxin analysis. This forms part of the master project of N. Abdullah.

Supplementary materials

Supplementary material associated with this article can be found, in the online version, at doi:10.1016/j.hal.2023.102475.

References

Anderson, D.M., Alpermann, T.J., Cembella, A.D., Collos, Y., Masseret, E., Montresor, M., 2012. The globally distributed genus *Alexandrium*: multifaceted roles in marine ecosystems and impacts on human health. Harmful Algae 14, 10–35. https://doi.org/10.1016/j.hal.2011.10.012.

Ankenbrand, M.J., Keller, A., Wolf, M., Schultz, J., Förster, F., 2015. ITS2 database V: twice as much. Mol. Biol. Evol. 32, 3030–3032. https://doi.org/10.1093/molbev/msv174.

Balech, E., 1985. The genus *Alexandrium* or *Gonyaulax* of the *tamarensis* group. In: Anderson, D.M., White, A.W., Baden, D.G. (Eds.), Toxic Dinoflagellates. Elsevier Publishers B.V, Amsterdam, pp. 33–38.

Balech, E., 1990. Four new dinoflagellates. Helgolander Meeresunters 44, 387–396.

Balech, E., 1995. The Genus *Alexandrium* Halim (Dinoflagellata). Sherkin Island Marine Station Publication, Sherkin Island, Co, Cork, Ireland.

Biecheler, B., 1952. Recherches sur les Péridiniens. Bull. Biol. France Belg. 36 (Suppl), 1–149.

Branco, S., Oliveira, M.M., Salgueiro, F., Vilar, M.C., Azevedo, S.M., Menezes, M., 2020. Morphology and molecular phylogeny of a new PST-producing dinoflagellate species: *alexandrium fragae* sp. nov. (Gonyaulacales, Dinophyceae). Harmful Algae 95, 101793.

Coleman, A.W., 2009. Is there a molecular key to the level of "biological species" in eukaryotes? A DNA guide. Mol. Phylogenet. Evol. 50 (1), 197–203.

Condie, S.A., Oliver, E.C.J., Hallegraeff, G.M., 2019. Environmental drivers of unprecedented *Alexandrium catenella* dinoflagellate blooms off eastern Tasmania, 2012–2018. Harmful Algae 87, 101628.

Darriba, D., Posada, D., 2014. jModelTest 2.0 Manual v0.1.1.

Darty, K., Denise, A., Ponty, Y., 2009. VARNA: interactive drawing and editing of the RNA secondary structure. Bioinformatics 25 (15), 1974.

Delgado, M., Garcés, E., Vila, M., Camp, J., 1997. Morphological variability in three populations of the dinoflagellate *Alexandrium taylori*. J. Plank. Res. 19 (6), 749757.

Díaz, P.A., Álvarez, G., Varela, D., Pérez-Santos, I., Díaz, M., Molinet, C., Seguel, M., Aguilera-Belmonte, A., Guzmán, L., Uribe, E., 2019. Impacts of harmful algal blooms on the aquaculture industry: chile as a case study. Perspect. Phycol. 6, 39–50.

Espiña, B., Cagide, E., Louzao, M.C., Vilariño, N., Vieytes, M.R., Takeda, Y., Sasaki, M., Botan, L.M., 2016. Cytotoxicity of goniodomin A and B in non contractile cells. Toxicol. Lett. 250–251, 10–20.

Fraga, S., Sampedro, N., Larsen, J., Moestrup, Ø, Calado, A.J., 2015. Arguments against the proposal 2302 by John & al. to reject the name *Gonyaulax catenella* (*Alexandrium catenella*). Taxon 64 (3), 634–635.

Gu, H., Zeng, N., Liu, T., Yang, W., Müller, A., Krock, B., 2013. Morphology, toxicity, and phylogeny of *Alexandrium* (Dinophyceae) species along the coast of China. Harmful Algae 27, 68–81.

Hallegraeff, G.M., 1993. A review of harmful algal blooms and their apparent global increase. Phycologia 32 (2), 79–99.

Hansen, G., Daugbjerg, N., Franco, J.M., 2003. Morphology, toxin composition and LSU rDNA phylogeny of *Alexandrium minutum* (Dinophyceae) from Denmark, with some morphological observations on other European strains. Harmful Algae 2 (4), 317–335.

Harding, J.M., Mann, R., Moeller, P.D.R., Hsia, M.H., 2009. Mortality of the veined rapa whelk, *Rapana venosa*, in relation to a bloom of *Alexandrium monilatum* in the York River, United States. J. Shellfish Res. 28, 363–367.

Harris, C.M., Krock, B., Tillmann, U., Tainter, C.J., Stec, D.F., Andersen, A.J.C., Larsen, T.O., Reece, K.S., Harris, T.M., 2021. Alkali metal and acid-catalyzed interconversion of goniodomin A with congeners B and C. J. Nat. Prod. 84, 2554–2567.

Hsia, M.H., Morton, S.L., Smith, L.L., Beauchesne, K.R., Muncik, K.M., Moeller, P.D.R., 2006. Production of goniodomin A by the planktonic, chain-forming dinoflagellate *Alexandrium monilatum* (Howell) Balech isolated from the Gulf Coast of the United States. Harmful Algae 5, 290–299.

Jin, D., Thunberg, E., Hoagland, P., 2008. Economic impact of the 2005 red tide event on commercial shellfish fisheries in New England. Ocean Coast. Manag. 51, 420–429.

John, U., Litaker, R.W., Montresor, M., Murray, S., Brosnahan, M.L., Anderson, D.M., 2014. Formal revision of the *Alexandrium tamarense* species complex (Dinophyceae) taxonomy: the introduction of five species with emphasis on molecular-based (rDNA) classification. Protist 165 (6), 779–804.

Keller, A., Schleicher, T., Schultz, J., Müller, T., Dandekar, T., Wolf, M., 2009. 5.8S-28S rRNA interaction and HMM-based ITS2 annotation. Gene 430, 50–57.

Kim, K.-Y., Yoshida, M., Kim, C.-H., 2005. Molecular phylogeny of three hitherto unreported Alexandrium species: *Alexandrium hiranoi, Alexandrium leei* and *Alexandrium satoanum* (Gonyaulacales, Dinophyceae) inferred from the 18S and 26S rDNA sequence data. Phycologia 44 (4), 361–368.

Kita, T., Fukuyo, Y., 1988. Description of the gonyaulacoid dinoflagellate Alexandrium hiranoi sp. nov. inhabiting tidepools on Japanese Pacific coast. Bull. Plankton Soc. Jap. 35 (1), 1–7.

Kremp, A., Hansen, P.J., Tillmann, U., Savela, H., Suikkanen, S., Voß, D., Barrera, F., Jakobsen, H.H., Krock, B., 2019. Distributions of three *Alexandrium* species and their toxins across a salinity gradient suggest an increasing impact of GDA producing *A. pseudogonyaulax* in shallow brackish waters of Northern Europe. Harmful Algae 87, 101622.

Kremp, A., Tahvanainen, P., Litaker, W., Krock, B., Suikkanen, S., Leaw, C.P., Tomas, C., 2014. Phylogenetic relationships, morphological variation, and toxin patterns in the *Alexandrium ostenfeldii* (Dinophyceae) complex: implications for species boundaries and identities. J. Phycol. 50, 81–100.

Krock, B., Tillmann, U., Wen, Y., Hansen, P.J., Larsen, T.O., Andersen, A.J.C., 2018. Development of a LC-MS/MS method for the quantification of goniodomins A and B and its application to *Alexandrium pseudogonyaulax* strains and plankton field samples of Danish coastal waters. Toxicon 155, 51–60.

Lê, S., Josse, J., Husson, F., 2008. FactoMineR: an R Package for multivariate analysis. J. Stat. Software 25 (1), 1–18.

Leaw, C.P., Lim, P.T., Ng, B.K., Cheah, M.Y., Ahmad, A., Usup, G., 2005. Phylogenetic analysis of *Alexandrium* species and *Pyrodinium bahamense* (Dinophyceae) based on theca morphology and nuclear ribosomal gene sequence. Phycologia 44 (5), 550–565.

Lilly, E.L., Halanych, K.M., Anderson, D.M., 2007. Species boundaries and global biogeography of the *Alexandrium tamarense* complex (Dinophyceae). J. Phycol. 43 (6), 1329–1338.

Lim, P.T., Sato, S., Van Thuoc, C., Tu, P.T., Huyen, N.T.M., , Takata, Yoshida, M., Kobiyama, A., Koike, K., Ogata, T., 2007. Toxic *Alexandrium minutum* (Dinophyceae) from Vietnam with new gonyautoxin analogue. Harmful Algae 6 (3), 321–331.

Lim, P.T., Usup, G., Leaw, C.P., 2012. Harmful algal blooms in Malaysian waters. Sains Malays 41 (12), 1509–1515.

Lim, P.T., Usup, G., Leaw, C.P., Ogata, T., 2005. First report of *Alexandrium taylori* and *Alexandrium peruvianum* (Dinophyceae) in Malaysia waters. Harmful Algae 4 (2), 391–400.

Lim, P.T., Yñiguez, A., Leaw, C.P., 2020. The toxic marine thecate dinoflagellate *Pyrodinium bahamense*. In: Shubba Rao, D.V. (Ed.), Dinoflagellates: Classification, Evolution, Physiology and Ecological Significance. Nova Science Publisher, pp. 481–498.

Litaker, R.W., Fraga, S., Montresor, M., Brosnahan, M., Anderson, D.M., Hoppenrath, M., Meer, S., Murray, S., Wolny, J., John, U., Sampedro, N., Larsen, J., Calado, A.J., 2018. A practical guide to new nomenclature for species within the "*Alexandrium tamarense* species complex. Harmful Algae News 61, 13–16.

Loeblich III, A., 1975. A seawater medium for dinoflagellates and the nutrition of *Cachonina niei*. J. Phycol. 11 (1), 80–86.

Long, M., Krock, B., Castrec, J., Tillmann, U., 2021. Unknown extracellular and bioactive metabolites of the genus *Alexandrium*: a review of overlooked toxins. Toxins (Basel) 13, 905.

Lundholm, N., Churro, C., Escalera, L., Fraga, S., Hoppenrath, M., Iwataki, M., Larsen, J., Mertens, K., Moestrup, Ø., Zingone, A., 2023. IOC-UNESCO taxonomic reference list of harmful micro algae. *Alexandrium* Halim 1960. Available online at. https://www.marinespecies.org/hab/aphia.php?p=taxdetails&id=109470. Accessed on 2023-06-06.

MacKenzie, L., de Salas, M., Adamson, J., Beuzenberg, V., 2004. The dinoflagellate genus *Alexandrium* (Halim) in New Zealand coastal waters: comparative morphology, toxicity and molecular genetics. Harmful Algae 3 (1), 71–92.

Mertens, K., et al., 2020. Morphological and phylogenetic data do not support the split of *Alexandrium* into four genera. Harmful Algae 98, 101902. https://doi.org/10.1016/j.hal.2020.101902.

Nagai, S., 2013. Species-specific detection of six *Alexandrium* species from single vegetative cells by a loop-mediated isothermal amplification method. DNA Testing 5, 33–46.

Nagai, S., Itakura, S., 2012. Specific detection of the toxic dinoflagellates *Alexandrium tamarense* and *Alexandrium catenella* from single vegetative cells by a loop-mediated isothermal amplification method. Mar. Genomics 7, 43–49.

Ronquist, F., Teslenko, M., van der Mark, P., Ayres, D.L., Darling, A., Höhna, S., Larget, B., Liu, L., Suchard, M.A., Huelsenbeck, J.P., 2012. MRBAYES 3.2: efficient Bayesian phylogenetic inference and model selection across a large model space. Syst. Biol. 61, 539–542.

Schliep, K.P., 2011. Phangorn: phylogenetic analysis in R. Bioinformatics 27 (4), 592–593.

Scholin, C.A., Herzog, M., Sogin, M., Anderson, D.M., 1994. Identification of group and strain-specific genetic markers for globally distributed *Alexandrium* (Dinophyceae). II. Sequence analysis of a fragment of the LSU rRNA gene. J. Phycol. 30, 999–1011.

Seibel, P.N., Müller, T., Dandekar, T., Wolf, M., 2008. Synchronous visual analysis and editing of RNA sequence and secondary structure alignments using 4SALE. BMC Res. Notes 1 (1), 1–7.

Swofford, D.L., 2001. PAUP* Phylogenetic Analysis Using Parsimony (*and Other Methods) Version 4.04beta. Sinauer Associates, Sunderland, Massachusetts.

Teng, S.T., Lim, H.C., Lim, P.T., Dao, V.H., Bates, S.S., Leaw, C.P., 2014. *Pseudo-nitzschia kodamae* sp. nov. (Bacillariophyceae), a toxigenic species from the Strait of Malacca, Malaysia. Harmful Algae 34, 17–28.

Teng, S.T., Tan, S.N., Lim, H.C., Dao, V.H., Bates, S.S., Leaw, C.P., 2016. High diversity of *Pseudo-nitzschia* along the northern coast of Sarawak (Malaysian Borneo), with descriptions of *P. bipertita* sp. nov. and *P. limii* sp. nov. (Bacillariophyceae). J. Phycol. 52 (6), 973–989.

Terao, K., Ito, E., Murakami, M., Yamaguchi, K., 1989. Histopathological studies on experimental marine toxin poisoning - III. Morphological changes in the liver and thymus of male ICR mice induced by Goniodomin A, isolated from the dinoflagellate *Goniodoma Pseudogoniaulax*. Toxicon 27, 269–271.

Tillmann, U., Bantle, A., Krock, B., Elbrächter, M., Gottschling, M., 2021. Recommendations for epitypification of dinophytes exemplified by *Lingulodinium polyedra* and molecular phylogenetics of the Gonyaulacales based on curated rRNA sequence data. Harmful Algae 104, 101956. https://doi.org/10.1016/j.hal.2020.101956.

Tillmann, U., John, U., 2002. Toxic effects of *Alexandrium* spp. on heterotrophic dinoflagellates: an allelochemical defence mechanism independent of PSP toxins. Mar. Ecol. Prog. Ser. 230, 47–58.

Tillmann, U., Krock, B., Wietkamp, S., Beran, A., 2020. A Mediterranean *Alexandrium taylorii* (Dinophyceae) strain produces Goniodomin A and lytic compounds but not paralytic shellfish toxins. Toxins (Basel) 12 (9), 564.

Trainer, V.L., 2020. GlobalHAB. Evaluating, reducing and mitigating the cost of harmful algal blooms: a compendium of case studies. PICES Sci. Rep., No. 59, 107.

Trainer, V.L., Yoshida, M., 2014. Proceedings of the workshop on economic impacts of harmful algal blooms on fisheries and aquaculture. PICES Sci. Rep., No. 47, 85pp.

Triki, H.Z., Laabir, M., Moeller, P., Chomérat, N., Daly-Yahia, O.K., 2016. First report of goniodomin A production by the dinoflagellate *Alexandrium pseudogonyaulax* developing in southern Mediterranean (Bizerte Lagoon, Tunisia). Toxicon 111, 91–99.

Usup, G., Leaw, C.P., Ahmad, A., Lim, P.T., 2002. Phylogenetic relationship of *Alexandrium tamiyavanichii* (Dinophyceae) to other *Alexandrium* species based on ribosomal RNA gene sequences. Harmful Algae 1, 59–68.

Wolf, M., Ruderisch, B., Dandekar, T., Schultz, J., Müller, T., 2008. ProfDistS:(profile-) distance based phylogeny on sequence-structure alignments. Bioinformatics 24 (20), 2401–2402.

Yñiguez, A.T., Lim, P.T., Leaw, C.P., Jipanin, S.J., Iwataki, M., Benico, G., Azanza, R.V., 2021. Over 30 years of HABs in the Philippines and Malaysia: what have we learned? Harmful Algae 102, 101776. https://doi.org/10.1016/j.hal.2020.101776.